

Radiatively Generated Parton Distributions of Real and Virtual Photons

M. Glück, E. Reya and I. Schienbein

*Institut für Physik, Universität Dortmund
D-44221 Dortmund, Germany*

Abstract

The parton content of real ($P^2 = 0$) and virtual ($P^2 \neq 0$) transverse photons $\gamma(P^2)$ is expressed in terms of perturbative pointlike and nonperturbative hadronic (VMD) components, employing recently updated parton distributions of pions and protons. The resulting parameter-free and perturbatively stable LO and NLO parton densities $f^{\gamma(P^2)}(x, Q^2)$ are smooth in P^2 and apply to all $P^2 \geq 0$ whenever $\gamma(P^2)$ is probed at scales $Q^2 \gg P^2$ where transverse photons also dominate physically relevant cross sections. Predictions are given for the structure function $F_2^{\gamma(P^2)}(x, Q^2)$ and $f^{\gamma(P^2)}(x, Q^2)$, and are compared with all relevant data for real photons as well as with recent data for virtual photons as extracted from DIS ep dijet events. Simple analytic parametrizations of our predicted parton distributions are presented for the real photon in LO and NLO, and for the virtual photon in LO which, within sufficient accuracy, may be also used in NLO-QCD.

1 Introduction

Modern theoretical QCD studies [1, 2, 3] of the parton distributions of real, i.e. on-shell, photons $f^\gamma(x, Q^2)$, $f = q, \bar{q}, g$, agree surprisingly well with measurements of the (anti) quark and gluon contents of the resolved real photons as obtained from e^+e^- and ep reactions at collider energies (for recent reviews, see [4, 5, 6]). For clarity let us denote the resolved real target photon with virtuality $P^2 \equiv -p^2 \simeq 0$ by $\gamma \equiv \gamma(P^2 \simeq 0)$ which is probed by the virtual probe photon $\gamma^*(Q^2)$, $Q^2 \equiv -q^2$, via the subprocess $\gamma^*(Q^2)\gamma \rightarrow X$ as in $e^+e^- \rightarrow e^+e^-X$. Here, p denotes the four-momentum of the photon emitted from, say, an electron in an e^+e^- or ep collider. In the latter case it is common to use Q^2 instead of P^2 for denoting the photon's virtuality, but we prefer P^2 for the subprocess $\gamma(P^2)p \rightarrow X$ according to the original notation used in e^+e^- annihilations. (Thus the factorization scale in $f^{\gamma(P^2)}(x, Q^2)$ refers now to some properly chosen scale of the produced hadronic system X , e.g. $Q \sim p_T^{\text{jet}}$ in high- p_T jet events, etc.).

In general one expects [7–12] also a virtual photon $\gamma(P^2 \neq 0)$ to possess a parton content $f^{\gamma(P^2)}(x, Q^2)$. It is a major problem to formulate a consistent set of boundary conditions which allow for a calculation of $f^{\gamma(P^2)}(x, Q^2)$ also in the next-to-leading order (NLO) of QCD as well as for a smooth transition to $P^2 = 0$, i.e. to the parton distributions of a real photon (see refs. [10, 11, 13] for a detailed discussion). Indeed, experimental studies of the transition of the deep inelastic (di-)jet cross section from the real photon to the virtual photon region at HERA point to the existence of a nonvanishing, though suppressed, parton content for virtual photons [14]. These measurements have triggered various analyses of the dependence of the ep jet production cross section on the virtuality of the exchanged photon [15, 16] and experimental tests of such predictions will elucidate the so far unanswered question as to when a deep inelastic scattering (DIS) ep process is eventually dominated by the usual ‘direct’ $\gamma^* \equiv \gamma(P^2)$ induced cross sections, not contaminated by the so far poorly known resolved virtual photon contributions. More recently, NLO calculations of the (di-)jet rate in ep (and eγ) scattering, which properly include the contributions of resolved virtual photons, have become available [17] and the

resolved virtual photon contributions have already been included in a Monte Carlo event generator [18] as well.

It is the main purpose of the present paper to formulate a consistent set of boundary conditions, utilizing our valence-like input parton distributions at the universal target-mass independent [1, 19, 20] low resolution scale $Q_0^2 = \mu^2 \simeq 0.3 \text{ GeV}^2$, which allow for a calculation of $f^{\gamma(P^2)}(x, Q^2)$ also in NLO-QCD as well as for a smooth transition to the parton distributions of a real photon, $P^2 = 0$. We shall furthermore employ the recently updated parton distributions of the pion [21], $f^\pi(x, Q^2)$, which are required for describing, via vector meson dominance (VMD), the hadronic components of the photon. It should be noted that the pionic gluon and sea densities, $g^\pi(x, Q^2)$ and $\bar{q}^\pi(x, Q^2)$, can be uniquely derived [21, 22] from the experimentally rather well known pionic valence density $v^\pi(x, Q^2)$ and the (also recently updated [23] dynamical) parton distributions $f(x, Q^2)$ of the proton. Thus we arrive at essentially parameter-free predictions for $f^{\gamma(P^2)}(x, Q^2)$ which are furthermore in good agreement with all present measurements of the structure function of real photons, $F_2^\gamma(x, Q^2)$.

In Sec. 2 we discuss the basic theoretical framework necessary for the presentation of our model for the parton distributions and structure functions of real photons, and compare the resulting predictions with recent experiments. Sec. 3 contains the formulation of our model for the parton distributions of virtual photons, together with some quantitative predictions for structure functions as well as a comparison with very recent data extracted from DIS dijet events. Our conclusions are drawn in Sec. 4. In the Appendix we present simple analytic parametrizations of our LO and NLO predictions for the parton distributions of real and virtual photons.

2 The Parton Content of Real Photons

High energy photons are mainly produced by the bremsstrahlung process $e(k) \rightarrow e(k') + \gamma(p)$. Here $p^2 = (k' - k)^2 = 2m_e^2 - 2k \cdot k'$ determines the virtuality of the produced photon which is declared as real (virtual) whenever $P^2 \equiv -p^2$ is smaller (larger) than some P_0^2 arbitrarily fixed experimentally (typically, $P_0^2 \simeq 10^{-2} \text{ GeV}^2$). Accordingly, the theoretical analysis is usually subdivided into two distinct parts corresponding to $P^2 \lesseqgtr P_0^2$. In terms of the photonic parton distributions, the structure function F_2^γ of a real photon $\gamma \equiv \gamma(P^2 \lesseqgtr P_0^2)$ is given in NLO($\overline{\text{MS}}$) QCD by

$$\begin{aligned} \frac{1}{x} F_2^\gamma(x, Q^2) &= \sum_q e_q^2 \left\{ q^\gamma(x, Q^2) + \bar{q}^\gamma(x, Q^2) \right. \\ &\quad \left. + \frac{\alpha_s(Q^2)}{2\pi} [C_q \otimes (q + \bar{q})^\gamma + 2C_g \otimes g^\gamma] + \frac{\alpha}{\pi} e_q^2 C_\gamma(x) \right\} \end{aligned} \quad (1)$$

where \otimes denotes the usual convolution integral. Here $\bar{q}^\gamma(x, Q^2) = q^\gamma(x, Q^2)$ and $g^\gamma(x, Q^2)$ provide the so-called ‘resolved’ contributions of γ to F_2^γ , while C_γ provides the ‘direct’ contribution as calculated according to the pointlike ‘box’ diagram $\gamma^*(Q^2)\gamma(P^2 \simeq 0) \rightarrow q\bar{q}$.

The Wilson coefficients [24] $C_{q,g}$ are given by

$$\begin{aligned} C_q(x) &= \frac{4}{3} \left[\frac{1+x^2}{1-x} \left(\ln \frac{1-x}{x} - \frac{3}{4} \right) + \frac{1}{4} (9 + 5x) \right]_+ \\ C_g(x) &= \frac{1}{2} \left[(x^2 + (1-x)^2) \ln \frac{1-x}{x} + 8x(1-x) - 1 \right], \end{aligned} \quad (2)$$

where the convolution with the $[]_+$ distribution can be easily calculated using, for example, eq. (A.21) of the first article in ref. [19], while the direct term in (1) is [25]

$$C_\gamma(x) = \frac{3}{(1/2)} C_g(x) = 3 \left[(x^2 + (1-x)^2) \ln \frac{1-x}{x} + 8x(1-x) - 1 \right]. \quad (3)$$

The appropriate coefficient function $C_{q,L}$ and $C_{g,L}$ for the longitudinal structure function $F_L^\gamma = F_2^\gamma - 2xF_1^\gamma$ may be found in [10].

In order to avoid the usual instabilities encountered in NLO($\overline{\text{MS}}$) in the large- x region due to the $\ln(1-x)$ term in (3), we follow ref. [1] and absorb such terms into the photonic $\overline{\text{MS}}$ quark distributions in (1): this results in the so-called DIS $_\gamma$ factorization scheme

which originally has been introduced for real photons by absorbing the entire C_γ term appearing in (1) into the NLO($\overline{\text{MS}}$) quark densities $\overset{(-)}{q}^\gamma(x, Q^2)$, i.e.

$$\begin{aligned} (q + \bar{q})_{\text{DIS}_\gamma}^\gamma &= (q + \bar{q})_{\overline{\text{MS}}}^\gamma + \frac{\alpha}{\pi} e_q^2 C_\gamma(x) \\ g_{\text{DIS}_\gamma}^\gamma &= g_{\overline{\text{MS}}}^\gamma \end{aligned} \quad (4)$$

with $C_\gamma(x)$ given by eq. (3). How much of the ‘finite’ terms in (3) is absorbed into the $\overline{\text{MS}}$ distributions in (4), is of course arbitrary and a matter of convention [3]. Since such different conventions [3, 5] turn out to be of minor importance for our quantitative results to be discussed below, we prefer to stick to the original DIS_γ scheme [1] as defined in eq. (4). Furthermore, the redefinition of the parton densities in (4) imply that the NLO($\overline{\text{MS}}$) splitting functions $k_{q,g}^{(1)}(x)$ of the photon into quarks and gluons, appearing in the inhomogeneous NLO RG evolution equations [1, 10] for $f^\gamma(x, Q^2)$, have to be transformed according to [1, 26]

$$\begin{aligned} k_q^{(1)}|_{\text{DIS}_\gamma} &= k_q^{(1)}|_{\overline{\text{MS}}} - e_q^2 P_{qq}^{(0)} \otimes C_\gamma \\ k_g^{(1)}|_{\text{DIS}_\gamma} &= k_g^{(1)}|_{\overline{\text{MS}}} - 2 \sum_q e_q^2 P_{gq}^{(0)} \otimes C_\gamma. \end{aligned} \quad (5)$$

The LO expression for F_2^γ is obviously entailed in eq. (1) by simply dropping all NLO terms proportional to $C_{q,g}$ as well as C_γ .

In NLO the expression for F_2^γ in the above DIS_γ factorization scheme is given by retaining the $C_{q,g}$ terms while dropping the destabilizing C_γ terms in eq. (1), which has already been absorbed into the quark densities according to eq. (4). Furthermore the nonperturbative hadronic VMD input $f^\gamma(x, Q_0^2)$ in NLO refers to the partons in the DIS_γ scheme which guarantees the perturbative stability of the resulting $F_2^\gamma(x, Q^2)$ provided this input is given by the NLO $f^\pi(x, Q_0^2)$ of [21], while the corresponding input in LO is given via VMD by the LO $f^\pi(x, Q_0^2)$ of [21]. We shall assume that the input resolution scale $Q_0^2 = \mu^2 \simeq 0.3 \text{ GeV}^2$ for the valence-like parton structure is universal, i.e. independent of the mass of the considered targets p, π, γ , etc. [1, 19, 20, 22]. The hadronic VMD ansatz

for $f^\gamma(x, \mu^2)$ is based on a coherent superposition of vector mesons [11]

$$|\gamma\rangle_{\mu^2, \text{had}} \simeq \frac{e}{f_\rho} |\rho\rangle_{\mu^2} + \frac{e}{f_\omega} |\omega\rangle_{\mu^2} \quad (6)$$

where the ϕ -meson contribution is considered to be strongly suppressed at $\mu^2 \ll m_\phi^2$. Assuming, within the operator product expansion (OPE),

$$\langle \rho | O_q | \rho \rangle_{\mu^2} = \langle \omega | O_q | \omega \rangle_{\mu^2} = 2 I_{3q} e^{-i\theta} \langle \rho | O_q | \omega \rangle_{\mu^2} = \langle \pi^0 | O_q | \pi^0 \rangle_{\mu^2} \quad (7)$$

$$\langle \rho | O_g | \rho \rangle_{\mu^2} = \langle \omega | O_g | \omega \rangle_{\mu^2} = \langle \pi^0 | O_g | \pi^0 \rangle_{\mu^2} \quad (8)$$

and $\langle \rho | O_g | \omega \rangle = 0$ due to isospin conservation, one obtains,

$$\begin{aligned} (u + \bar{u})^\gamma(x, \mu^2) &= \alpha(g_\rho^2 + g_\omega^2 + 2g_\rho g_\omega \cos \theta)(u + \bar{u})^{\pi^0}(x, \mu^2) \\ (d + \bar{d})^\gamma(x, \mu^2) &= \alpha(g_\rho^2 + g_\omega^2 - 2g_\rho g_\omega \cos \theta)(d + \bar{d})^{\pi^0}(x, \mu^2) \\ (s + \bar{s})^\gamma(x, \mu^2) &= \alpha(g_\rho^2 + g_\omega^2)(s + \bar{s})^{\pi^0}(x, \mu^2) = 0 \\ g^\gamma(x, \mu^2) &= \alpha(g_\rho^2 + g_\omega^2)g^{\pi^0}(x, \mu^2). \end{aligned} \quad (9)$$

Here $O_{q,g}$ refer to the leading twist-2 quark and gluon operators in the OPE formalism, $g^\gamma \equiv \langle \gamma | O_g | \gamma \rangle_{\text{had}}$ etc., and $g_V^2 \equiv 4\pi/f_V^2$ with

$$g_\rho^2 = 0.50, \quad g_\omega^2 = 0.043, \quad (10)$$

i.e. $f_\rho^2/4\pi = 2.0$ and $f_\omega^2/4\pi = 23.26$, as obtained from a zero-width calculation of the relevant leptonic widths $\Gamma(V \rightarrow \ell^+ \ell^-) = \alpha^2 m_V g_V^2 / 3$ presented in [27]. The omission of a finite-width correction for g_ρ^2 is due to the central role [27] of the precise results in [28] which do not require such a correction in contrast to the situation for the less precise resonance analysis at e^+e^- colliders [29].

For the a priori unknown coherence factor (fit parameter) $\cos \theta$ in eq. (9) we take $\cos \theta = 1$, i.e. we favor a superposition of u and d quarks which maximally enhances the contributions of the up-quarks to F_2^γ in eq. (1). This favored value for $\cos \theta$ is also supported by fitting $\cos \theta$ in (9) to all presently available data on $F_2^\gamma(x, Q^2)$, to be discussed below, which always resulted in $\cos \theta \simeq 1$ in LO as well as NLO. This is also in

agreement with the LO results obtained in ref. [11]. The LO and NLO input distributions $f^\pi(x, \mu^2)$ of the pion in (9) are taken from a recent analysis [21] which correspond to [21, 23] $\mu_{\text{LO}}^2 = 0.26 \text{ GeV}^2$ and $\mu_{\text{NLO}}^2 = 0.40 \text{ GeV}^2$ in LO and NLO, respectively. Since by now all free input quantities have been fixed in eq. (9), we arrive at rather unique parameter-free predictions for $f^\gamma(x, Q^2)$ and $F_2^\gamma(x, Q^2)$.

The calculation of $f^\gamma(x, Q^2)$ at $Q^2 > \mu^2$ follows from the well known inhomogeneous RG evolution equations in LO and NLO (see, for example, [1, 26]) which we solve, as usual, analytically for the n -th Mellin moment of $f^\gamma(x, Q^2)$, followed by a straightforward Mellin-inversion to Bjorken- x space. The explicit formal solutions can be found in eqs. (2.12) and (2.13) of the first article of ref. [1]. The general structure of these solutions is

$$f^\gamma(x, Q^2) = f_{pl}^\gamma(x, Q^2) + f_{\text{had}}^\gamma(x, Q^2). \quad (11)$$

Here f_{pl}^γ denotes the perturbative ‘pointlike’ solution which vanishes at $Q^2 = \mu^2$ and is driven by the pointlike photon splitting functions $k_{q,g}^{(0,1)}(x)$ appearing in the inhomogeneous evolution equations, while f_{had}^γ depends on the hadronic input $f^\gamma(x, \mu^2)$ in eq. (9) and evolves according to the standard homogeneous evolution equations. We treat these solutions in precisely the same way as discussed in detail in [10], except that we implement an improved treatment of the running $\alpha_s(Q^2)$ by exactly solving in NLO($\overline{\text{MS}}$)

$$\frac{d\alpha_s(Q^2)}{d\ln Q^2} = -\frac{\beta_0}{4\pi} \alpha_s^2(Q^2) - \frac{\beta_1}{16\pi^2} \alpha_s^3(Q^2) \quad (12)$$

numerically [23] using $\alpha_s(M_Z^2) = 0.114$, rather than using the usual approximate NLO solution (e.g. eq. (14) in [10]) which becomes sufficiently accurate only for $Q^2 \gtrsim m_c^2 \simeq 2 \text{ GeV}^2$ [23]. Here, $\beta_0 = 11 - 2f/3$ and $\beta_1 = 102 - 38f/3$.

The prescription for the VMD ansatz in eq. (9) at the input scale μ^2 , together with $\cos\theta = 1$ as discussed above, yields a simple expression for the general Q^2 -dependence of $f^\gamma(x, Q^2)$:

$$f^\gamma(x, Q^2) = f_{pl}^\gamma(x, Q^2) + \alpha \left[G_f^2 f^\pi(x, Q^2) + \delta_f \frac{1}{2} (G_u^2 - G_d^2) s^\pi(x, Q^2) \right] \quad (13)$$

with $\delta_u = -1$, $\delta_d = +1$ and $\delta_s = \delta_g = 0$, and where the index π obviously refers to π^0 and

$$\begin{aligned}
G_u^2 &= (g_\rho + g_\omega)^2 \simeq 0.836 \\
G_d^2 &= (g_\rho - g_\omega)^2 \simeq 0.250 \\
G_s^2 &= G_g^2 = g_\rho^2 + g_\omega^2 = 0.543.
\end{aligned} \tag{14}$$

Simple analytic LO and NLO(DIS $_\gamma$) parametrizations for the pointlike piece $f_{pl}^\gamma(x, Q^2)$ are given in the Appendix, whereas the ones for $f^\pi(x, Q^2)$ can be found in [21].

The photonic quark distributions discussed thus far and which appear in eq. (1) are adequate for the $f = 3$ light u, d, s flavors. Since heavy quarks $h = c, b, t$ will not be considered as ‘light’ partons in the photon (as in the case of the proton [23] and the pion [21, 22]), their contributions to F_2^γ have to be calculated in fixed order perturbation theory according to the ‘direct’ box–diagram $\gamma^*(Q^2)\gamma \rightarrow h\bar{h}$ expression, i.e. the usual Bethe–Heitler cross section [30]

$$\begin{aligned}
\frac{1}{x} F_{2,h}^\gamma(x, Q^2) &= 3 e_h^4 \frac{\alpha}{\pi} \theta(\beta^2) \left\{ \beta \left[8x(1-x) - 1 - x(1-x) \frac{4m_h^2}{Q^2} \right] \right. \\
&\quad \left. + \left[x^2 + (1-x)^2 + x(1-3x) \frac{4m_h^2}{Q^2} - x^2 \frac{8m_h^4}{Q^4} \right] \ln \frac{1+\beta}{1-\beta} \right\} \tag{15}
\end{aligned}$$

where $\beta^2 \equiv 1 - 4m_h^2/W^2 = 1 - 4m_h^2x/(1-x)Q^2$. This expression has to be added to eq. (1) and a similar expression holds for the longitudinal structure function [10] $F_L \equiv F_2 - 2xF_1$. The ‘resolved’ heavy quark contribution [10] to F_2^γ in (1) has to be calculated via $\gamma^*(Q^2)g^\gamma \rightarrow h\bar{h}$,

$$F_{2,h}^{g^\gamma}(x, Q^2) = \int_{z_{\min}}^1 \frac{dz}{z} z g^\gamma(z, \mu_F^2) f_2^{\gamma^*(Q^2)g^\gamma \rightarrow h\bar{h}}\left(\frac{x}{z}, Q^2\right) \tag{16}$$

where $\frac{1}{x} f_2^{\gamma^*(Q^2)g^\gamma \rightarrow h\bar{h}}(x, Q^2)$ is given by eq. (15) with $e_h^4 \alpha \rightarrow e_h^2 \alpha_s(\mu_F^2)/6$, $z_{\min} = x(1 + 4m_h^2/Q^2)$ and $\mu_F^2 \simeq 4m_h^2$ [31]. This ‘resolved’ LO contribution should be included in eq. (1) as well. To ease the calculations we shall keep these LO expressions (15) and (16) also in NLO, since the full NLO expressions for heavy quark production [32] turn out to be a small correction to the already not too sizeable (at most about 20%) contribution in LO. Notice that such small corrections are not larger than ambiguities due to different

choices for m_h and for the factorization scale μ_F . For our purposes it is sufficient to include only the charm contributions which will be calculated using $m_c = 1.4$ GeV.

Having outlined the theoretical basis for our photonic parton distributions, we now turn to the quantitative results. First we apply our parameter-free predictions for $f^\gamma(x, Q^2)$ to the structure function of real photons which, according to eq. (1) and the above results, is finally given by

$$\begin{aligned} \frac{1}{x} F_2^\gamma(x, Q^2) = & 2 \sum_{q=u,d,s} e_q^2 \left\{ q^\gamma(x, Q^2) + \frac{\alpha_s(Q^2)}{2\pi} [C_q \otimes q^\gamma + C_g \otimes g^\gamma] \right. \\ & \left. + \frac{1}{x} F_{2,c}^\gamma(x, Q^2) + \frac{1}{x} F_{2,c}^{g^\gamma}(x, Q^2) \right\} \end{aligned} \quad (17)$$

where $f^\gamma(x, Q^2)$ refers to the DIS $_\gamma$ factorization scheme defined in (4) and the charm contributions $F_{2,c}^{\gamma(P^2)}$ and $F_{2,c}^{g^\gamma}$ are given by eqs. (15) and (16), respectively. In fig. 1 we compare our LO and NLO predictions with all available relevant data [33] for F_2^γ of the real photon. Our present new NLO results are rather similar to the ones of AFG [3], but differ from our previous (GRV $_\gamma$) predictions [1] which are steeper in the small- x region, as shown in fig. 1, because the dominant hadronic (pionic) sea density $\bar{q}^\pi(x, Q^2)$ is steeper since it has been generated purely dynamically from a vanishing input at $Q^2 = \mu^2$ [1, 20]. Similarly the SaS 1D [11] expectations, for example, fall systematically below the data in the small to medium Q^2 region around $Q^2 \simeq 5$ GeV 2 , partly due to a somewhat different treatment of the hadronic coherent VMD input as compared to our results in eqs. (9) and (13) and (14). The relevant LO and NLO photonic parton densities are compared in fig. 2 at $Q^2 = 10$ GeV 2 . For illustration we also show the purely ‘hadronic’ component (homogeneous solution) in (11) of f^γ which demonstrates the dominance of the ‘pointlike’ component (inhomogeneous solution) in (11) for u^γ and d^γ in the large- x region, $x > 0.1$. In fig. 3 we show our predictions for $xu^\gamma(x, Q^2)$ and $xg^\gamma(x, Q^2)$. The parton distributions of the photon behave, in contrast to the ones of a hadron, very differently in the limits of large and small x . In the former case, the purely perturbative pointlike part in (11) dominates for $x \gtrsim 0.1$, especially for the quark distributions. On the other hand, this uniquely calculable contribution amounts at most to about 20% at very small x where the hadronic VMD component in (11) dominates, giving rise to a

very similar increase for $x \rightarrow 0$ as observed in the proton case. In fig. 3 we also show our valence-like inputs at $Q^2 = \mu_{\text{LO,NLO}}^2$ which become (vanishingly) small at $x < 10^{-2}$. This illustrates the purely dynamical origin of the small- x increase at $Q^2 > \mu^2$. Also noteworthy is the perturbative LO/NLO stability of $u^\gamma(x, Q^2)$ which is almost as good as the one required for a physical quantity like $F_2^\gamma(x, Q^2)$ in fig. 1. The situation is, as usual [1, 19, 23], different for $g^\gamma(x, Q^2)$. Nevertheless, despite the sizable difference between the LO and NLO gluon distributions in fig. 3 in the small- x region, the directly measurable F_2^γ and the gluon-dominated heavy quark contribution in eq. (16) shows a remarkable perturbative stability [23]. Finally, we compare in fig. 4 our predictions for $xg^\gamma(x, Q^2)$ at $Q^2 \equiv (p_T^{\text{jet}})^2 = 75 \text{ GeV}^2$ with recent HERA (H1) measurements [34]. Our somewhat flatter results for xg^γ in the small- x region, as compared to the older GRV_γ expectations [1], is caused by the recently favored flatter gluon distribution in the proton [23] which determines g^γ via g^π [21], cf. eq. (9), at small x .

Finally it is interesting to consider the total momenta carried by the photonic partons,

$$M_2^\gamma(Q^2) \equiv \sum_{f=q,\bar{q},g} \int_0^1 x f^\gamma(x, Q^2) dx. \quad (18)$$

Inspired by the ideas and suggestions put forward in refs. [35, 11], it has been conjectured recently [36] that this leading twist-2 quantity M_2^γ should satisfy, in LO-QCD,

$$M_2^\gamma(Q^2) \simeq \Pi_h(Q^2) \quad (19)$$

where the well known dispersion relation relates the hadronic part of the photon's vacuum polarization

$$\Pi_h(Q^2) = \frac{Q^2}{4\pi^2\alpha} \int_{4m_\pi^2}^\infty \frac{\sigma_h(s)}{s + Q^2} ds \quad (20)$$

to $\sigma_h \equiv \sigma(e^+e^- \rightarrow \text{hadrons})$. It should be noted that $\Pi_h(Q^2)$, being an experimental quantity, includes, besides the usual twist-2 term, all possible nonperturbative higher-twist contributions. The 'consistency' relation (19) is, however, expected to hold already at $Q^2 \gtrsim 2$ to 4 GeV^2 to within, say, 20 to 30% where the twist-2 component in $\Pi_h(Q^2)$ may become dominant, as possibly indicated by DIS ep processes. Indeed, our LO results

imply $M_2^\gamma(2 \text{ GeV}^2)/\alpha \simeq 0.976$ and $M_2^\gamma(4 \text{ GeV}^2)/\alpha \simeq 1.123$ which compares favorably with [37] $\Pi_h(2 \text{ GeV}^2)/\alpha = 0.694 \pm 0.028$ and $\Pi_h(4 \text{ GeV}^2)/\alpha = 0.894 \pm 0.036$, respectively.

3 The Parton Content of Virtual Photons

Next we turn to the somewhat more speculative concept and models of ‘resolved’ virtual photons ($P^2 \neq 0$). The real photons considered in Section 2 are those whose virtuality P^2 is very small, i.e. of the order $P_{min}^2 = \mathcal{O}(m_e^2)$ or, experimentally, at least $P^2 < P_0^2 \simeq 10^{-2} \text{ GeV}^2$. The flux of virtual photons produced by the bremsstrahlung process $e(k) \rightarrow e(k') + \gamma(p)$, $P^2 \equiv -p^2 = -(k' - k)^2 > P_0^2$ is given by [38]

$$f_{\gamma(P^2)/e}^T(y) = \frac{\alpha}{2\pi} \left[\frac{1 + (1-y)^2}{y} \frac{1}{P^2} - \frac{2m_e^2 y}{P^4} \right] \quad (21)$$

$$f_{\gamma(P^2)/e}^L(y) = \frac{\alpha}{2\pi} \frac{2(1-y)}{y} \frac{1}{P^2} \quad (22)$$

with $y = E_\gamma/E_e$ and $T(L)$ denoting transverse (longitudinal) photons. Whenever these virtual photons, with their virtuality being entirely taken care of by the flux factors in (21) and (22), are probed at a scale $Q^2 \gg P^2$ they may be considered as real photons which means that [7, 8, 12, 15, 16, 17]

- (i) effects due to $f_{\gamma(P^2)/e}^L$ should be neglected since the corresponding longitudinal cross sections are suppressed by powers of P^2/Q^2 ;
- (ii) cross sections of partonic subprocesses involving $\gamma(P^2)$ should be calculated as if $P^2 = 0$ due (partly) to the P^2/Q^2 power suppressions of any additional terms.

This latter rule implies in particular that the NLO ‘direct’ contribution $C_{\gamma(P^2)}(x)$ to $F_2^{\gamma(P^2)}(x, Q^2)$ has to be the same $C_\gamma(x)$ as for real photons in eqs. (1) and (3), i.e. has to be inferred from the real photon subprocess $\gamma^*(Q^2)\gamma \rightarrow q\bar{q}$, and not from the doubly-virtual box $\gamma^*(Q^2)\gamma(P^2) \rightarrow q\bar{q}$ as originally proposed [7, 8] and used [10]. Thus we can implement the same DIS_γ factorization scheme as for real photons in eq. (4), and the

structure function of virtual photons becomes formally very similar to eq. (17):

$$\begin{aligned} \frac{1}{x} F_2^{\gamma(P^2)}(x, Q^2) &= 2 \sum_{q=u,d,s} e_q^2 \left\{ q^{\gamma(P^2)}(x, Q^2) + \frac{\alpha_s(Q^2)}{2\pi} [C_q \otimes q^{\gamma(P^2)} + C_g \otimes g^{\gamma(P^2)}] \right. \\ &\quad \left. + \frac{1}{x} F_{2,c}^{\gamma}(x, Q^2) + \frac{1}{x} F_{2,c}^{g\gamma(P^2)}(x, Q^2) \right\} \end{aligned} \quad (23)$$

with $C_{q,g}(x)$ given in (2). The ‘direct’ heavy (charm) quark contribution is given by eq. (15) as for real photons since $F_{2,c}^{\gamma(P^2)} = F_{2,c}^{\gamma}$ as follows from our consistent strict adherence to point (ii) above. The ‘resolved’ charm contribution $F_{2,c}^{g\gamma(P^2)}$ is as in eq. (16) with the gluon distribution $g^{\gamma}(z, \mu_F^2) \rightarrow g^{\gamma(P^2)}(z, \mu_F^2)$.

The above consistency requirements afford furthermore the following boundary conditions for $f^{\gamma(P^2)}$, cf. eq. (13),

$$f^{\gamma(P^2)}(x, Q^2 = \tilde{P}^2) = f_{\text{had}}^{\gamma(P^2)}(x, \tilde{P}^2) = \eta(P^2) f_{\text{had}}^{\gamma}(x, \tilde{P}^2) \quad (24)$$

in LO as well as in NLO. Here $\tilde{P}^2 = \max(P^2, \mu^2)$ as dictated by continuity in P^2 [10] and $\eta(P^2) = (1 + P^2/m_\rho^2)^{-2}$ is a dipole suppression factor with $m_\rho^2 = 0.59 \text{ GeV}^2$. The second equality in eq. (24) follows from the consistency requirement $C_{\gamma(P^2)} = C_\gamma$ and consequently the application of the same $\overline{\text{MS}} \rightarrow \text{DIS}_\gamma$ factorization scheme transformation as for the real photon, cf. eq. (23). The scale \tilde{P}^2 is dictated not only by the above mentioned continuity requirement, but also by the fact that the hadronic component of $f^{\gamma(P^2)}(x, Q^2)$ is probed at the scale $Q^2 = \tilde{P}^2$ [9, 10, 11] where the pointlike component vanishes by definition. The boundary condition in eq. (24) guarantees, as should be evident, a far better perturbative stability as compared to the situation in [10] where the NLO input differed drastically from its LO counterpart (cf. eq. (8) in ref. [10]).

The evolution to $Q^2 > \tilde{P}^2$ is now analogous to the case of real photons in the previous section and the general solution for the resulting parton distributions is similar to the one in eq. (11) and eq. (13),

$$\begin{aligned} f^{\gamma(P^2)}(x, Q^2) &= f_{pl}^{\gamma(P^2)}(x, Q^2) + f_{\text{had}}^{\gamma(P^2)}(x, Q^2) \\ &= f_{pl}^{\gamma(P^2)}(x, Q^2) + \eta(P^2) \alpha \left[G_f^2 f^\pi(x, Q^2) + \delta_f \frac{1}{2} (G_u^2 - G_d^2) s^\pi(x, Q^2) \right] \end{aligned} \quad (25)$$

with δ_f as in eq. (13) and where $f_{\text{had}}^{\gamma(P^2)}$ refers again to the solution of the homogeneous RG evolution equations, being driven by the hadronic input in (24), which is explicitly given by eq. (13) of ref. [10]. Its parametrization is fixed by the available parametrization [21] for $f^\pi(x, Q^2)$ in (25). The inhomogeneous ‘pointlike’ solution in (25) is explicitly given by eq. (12) of [10] where $L = \alpha_s(Q^2)/\alpha_s(\tilde{P}^2)$. A parametrization of $f_{pl}^{\gamma(P^2)}(x, Q^2)$ in LO is thus easily obtained from the one for the real photon $f_{pl}^\gamma(x, Q^2)$ in (13) in terms of $\ln L^{-1} = \ln [\alpha_s(\mu^2)/\alpha_s(Q^2)]$, where now $\alpha_s(\mu^2)$ has simply to be replaced by $\alpha_s(\tilde{P}^2)$ as described in detail in Appendix 1. Furthermore, since our NLO predictions for $f^{\gamma(P^2)}(x, Q^2)$ turn out to be rather similar to the LO ones, as will be shown below, the simple analytic LO parametrizations for $f^{\gamma(P^2)}(x, Q^2)$ can be used for NLO calculations as well. This is certainly sufficiently accurate and reliable in view of additional model ambiguities inherent in the parton distributions of virtual photons.

It should be emphasized that the RG resummed results in (25) are relevant whenever $P^2 \ll Q^2$, typically [10, 15] $P^2 \simeq \frac{1}{10} Q^2$, so as to suppress power-like (possibly higher twist) terms $(P^2/Q^2)^n$ which would spoil the dominance of the resummed logarithmic contributions and, furthermore, to guarantee the dominance of the transverse photon contributions (21) to physical cross sections. For P^2 approaching Q^2 , the $e^+e^- \rightarrow e^+e^-X$ reaction, for example, should be simply described by the full fixed order box $\gamma^*(Q^2)\gamma(P^2) \rightarrow q\bar{q}$ keeping all $(P^2/Q^2)^n$ terms. Since the full perturbative $\mathcal{O}(\alpha_s)$ corrections to this virtual box have not been calculated yet, it is not possible, for the time being, to determine reliably at what values of P^2 (and possibly x) this $\mathcal{O}(\alpha_s)$ corrected virtual box becomes the more appropriate and correct description. Similar remarks hold for a DIS process $ep \rightarrow eX$, i.e. $\gamma(P^2)p \rightarrow X$, where $\mathcal{O}(\alpha_s)$ corrections to pointlike virtual $\gamma(P^2)$ -parton subprocesses have to be analyzed in detail in order to decide at what P^2 these pointlike expressions become the more appropriate description and the virtual photonic parton distributions (i.e., resummations) become irrelevant.

Our strict adherence to the above point (ii) implies that the ‘direct’ photon contribution to any process whatsoever should always be calculated as if this photon is

real apart from the fact that its flux should be evaluated according to eq. (21) with $P^2 \neq 0$ [12, 15, 16]. This differs from the somewhat inconsistent procedure adopted by the HERA–H1 collaboration [14] where exact $eq \rightarrow eqg$ and $eg \rightarrow eq\bar{q}$ matrix elements were used for the direct photon contribution to the dijet cross section. As long as $P^2 \lesssim \frac{1}{10} Q^2$, the exact treatment of matrix elements, however, should not differ too much [17] from the more appropriate treatment described above. To conclude let us stress that the strict adherence to point (ii), as illustrated by the foregoing examples, is not a free option but a necessary consistency condition for introducing the concept of the resolved parton content of the virtual photon as an alternative to a non-resummed fixed order perturbative analysis at $P^2 \neq 0$. This consistency requirement is related to the fact that all the resolved contributions due to $f^{\gamma(P^2)}(x, Q^2)$ are calculated (evolved) as if these partons are massless [7 – 11] (i.e. employing photon splitting functions for real photons, etc.) in spite of the fact that their actual virtuality is given by $P^2 \neq 0$. Thus the direct photon contribution should obviously be also treated accordingly.

Now we turn to our quantitative predictions and first compare our results with the old PLUTO measurements [39] for $F_{\text{eff}}^{\gamma(P^2)}(x, Q^2) \equiv F_2^{\gamma(P^2)} + \frac{3}{2}F_L^{\gamma(P^2)}$ in fig. 5. Our very similar LO and NLO results, which are dominated by the almost unique ‘pointlike’ contribution in (25), are in full agreement with the limited poor statistics of the PLUTO data. The GRS [10] expectations turn out to be very similar to our present ones shown in fig. 5. For illustration the naive (i.e. not resummed) LO quark–parton model ‘box’ expectation is shown as well by the dotted curve in fig. 5 which is given by

$$\frac{1}{x} F_{2,\text{box}}^{\gamma(P^2)}(x, Q^2) = 3 \sum_{q=u,d,s} e_q^4 \frac{\alpha}{\pi} [x^2 + (1-x)^2] \ln \frac{Q^2}{P^2} + \frac{1}{x} F_{2,c}^{\gamma(P^2)}(x, Q^2) \quad (26)$$

$$\frac{1}{x} F_{L,\text{box}}^{\gamma(P^2)}(x, Q^2) = 3 \sum_{q=u,d,s} e_q^4 \frac{\alpha}{\pi} 4x(1-x) + \frac{1}{x} F_{L,c}^{\gamma(P^2)}(x, Q^2) \quad (27)$$

with the heavy quark (charm) contribution $F_{2,c}^{\gamma(P^2)}$ given by eq. (15) and

$$\frac{1}{x} F_{L,c}^{\gamma(P^2)}(x, Q^2) = 3 e_c^4 \frac{4\alpha}{\pi} \left[\beta x(1-x) - x^2 \frac{2m_c^2}{Q^2} \ln \frac{1+\beta}{1-\beta} \right]. \quad (28)$$

More detailed predictions for $F_2^{\gamma(P^2)}(x, Q^2)$ are presented in figs. 6a and 6b for various virtualities P^2 and scales Q^2 . Since the ‘pointlike’ component in (25) is uniquely calculable perturbatively, a detailed measurement of the x and P^2 dependence at various fixed values of Q^2 , as shown in figs. 6a and 6b, would shed light on the theoretically more speculative and far less understood nonperturbative ‘hadronic’ contribution in eq. (25) and eventually establish the absolute perturbative predictions. Our LO and NLO predictions in figs. 6a and 6b show a remarkable perturbative stability throughout the whole x -region shown, except perhaps for $P^2 \gg 1 \text{ GeV}^2$ where the perturbatively very stable [21, 22] ‘hadronic’ component in (25) becomes strongly suppressed with respect to the ‘pointlike’ solution which is less stable in the small x region, $x < 10^{-2}$, as is evident from fig. 6b.

The individual LO and NLO parton distributions of the virtual photon at $Q^2 = 10 \text{ GeV}^2$ are shown in fig. 7a where they are compared with the ones of GRS [10]. The LO SaS expectations [11] are compared with our LO predictions in fig. 7b. In figs. 8 and 9 we show our predictions for $xu^{\gamma(P^2)}(x, Q^2)$ and $xg^{\gamma(P^2)}(x, Q^2)$ with particular emphasis on the very small x region. For comparison we also show the results for a real ($P^2 = 0$) photon. Plotting the ‘hadronic’ component in (25) separately in fig. 8 demonstrates that the perturbative ‘pointlike’ component in (25) dominates for $x > 10^{-2}$. Furthermore the expected perturbative stability of our present LO and NLO predictions is fulfilled. This is in contrast to the GRS results which are unstable [10] throughout the whole x -region for $P^2 \gtrsim 1 \text{ GeV}^2$, as illustrated in fig. 9 at $Q^2 = 100 \text{ GeV}^2$, due to the very different perturbative (box) input in LO and NLO [10]. In general, however, as soon as the perturbatively very stable ‘hadronic’ component in (25) becomes suppressed for $P^2 \gg 1 \text{ GeV}^2$, the remaining perturbatively less stable ‘pointlike’ component destabilizes the total results for $q^{\gamma(P^2)}(x, Q^2)$ in the very small x region, $x \lesssim 10^{-3}$, as can be seen in fig. 9 for $u^{\gamma(P^2)}$ at $Q^2 = 100 \text{ GeV}^2$ (cf. fig. 6b).

Finally in fig. 10 we confront our LO predictions for $f^{\gamma(P^2)}(x, Q^2)$ with the effective parton density

$$\tilde{f}^{\gamma(P^2)}(x, Q^2) = \sum_{q=u,d,s} \left(q^{\gamma(P^2)} + \bar{q}^{\gamma(P^2)} \right) + \frac{9}{4} g^{\gamma(P^2)} \quad (29)$$

extracted in LO from DIS dijet data by the HERA–H1 collaboration [14] very recently. The predicted dependence on the photon’s virtuality P^2 at the scale $Q^2 \equiv (p_T^{\text{jett}})^2 = 85 \text{ GeV}^2$ agrees reasonably well with the measurements in the relevant kinematic region $P^2 \ll Q^2$. This is also the case at other scales $Q^2 \equiv (p_T^{\text{jett}})^2$ and fixed values of x [14] not shown in fig. 10. As discussed above, it should be kept in mind, however, that for larger values of P^2 approaching Q^2 , which refer to the dashed curves in fig. 10, the whole concept of RG resummed parton distributions of virtual photons is not appropriate anymore. Since the resolved contributions of a virtual photon with virtuality as large as $P^2 = 10 - 15 \text{ GeV}^2$ are by a factor of about 10 smaller than the ones of a real ($P^2 = 0$) photon, it is reasonable to conclude from fig. 10 that for $P^2 \gtrsim 10 \text{ GeV}^2$ the DIS $ep \rightarrow eX$ process considered is dominated by the usual direct $\gamma^* \equiv \gamma(P^2)$ exchange cross sections and not ‘contaminated’ anymore by resolved contributions. This furthermore explains the trend of the discrepancies between the data and our as well as other [11, 12] predictions which can be traced to the fact that the direct photon contributions were not calculated as if $\gamma^*(P^2)$ was real, as required by our consistency condition (ii). Thus the direct photon contribution was likely underestimated, particularly at the larger value of x , $x = 0.6$, resulting in an overestimate of $x\tilde{f}^{\gamma(P^2)}(x, Q^2)$ at $P^2 \gtrsim 5 \text{ GeV}^2$.

4 Summary and Conclusions

The main purpose of the present paper was to formulate a consistent set of boundary conditions which allow for a perturbatively stable LO and NLO calculation of the photonic parton distributions $f^{\gamma(P^2)}(x, Q^2)$ as well as for a smooth transition to the parton densities of a real ($P^2 = 0$) photon. Employing the recently updated [21] pionic distributions $f^\pi(x, Q^2)$, required for describing, via VMD, the nonpointlike hadronic components of a photon, we arrive at essentially parameter–free predictions for $f^{\gamma(P^2)}(x, Q^2)$ which are furthermore in good agreement with all present measurements of the structure function $F_2^\gamma(x, Q^2)$ of real photons $\gamma \equiv \gamma(P^2 = 0)$. It should be noted that the experimentally almost unconstrained pionic gluon and sea distributions, $g^\pi(x, Q^2)$ and $\bar{q}^\pi(x, Q^2)$, have

been uniquely derived [21, 22] from the experimentally rather well known pionic valence density $v^\pi(x, Q^2)$ and the (also recently updated [23] dynamical) parton distributions of the proton. We have furthermore implemented these hadronic components by using a VMD ansatz for a coherent superposition of vector mesons which maximally enhances the contributions of the up-quarks to F_2^γ as favored by all present data. Since these hadronic contributions are generated from the valence-like input parton distributions at the universal target-mass independent low resolution scale $Q_0^2 = \mu^2 \simeq 0.3 \text{ GeV}^2$, we arrive, at least for real ($P^2 = 0$) photons, at unique small- x predictions for $x \lesssim 10^{-2}$ at $Q^2 > \mu^2$ which are of purely dynamical origin, as in the case of hadrons. Furthermore, since our universal input scale μ^2 fixes also uniquely the perturbative pointlike part of the photonic parton distributions, which dominates for $x \gtrsim 0.1$, the large- x behavior of photonic structure functions is unambiguously predicted as well.

Our expectations for the parton content of virtual ($P^2 \neq 0$) photons are clearly more speculative, depending on how one models the hadronic component (input) of a virtual photon. The latter is usually assumed to be similar to the VMD input for a real photon, times a dipole suppression factor which derives from an effective vector-meson P^2 -propagator, cf. eq. (24). Whenever a virtual photon is probed at a scale $Q^2 \gg P^2$, with its virtuality being entirely taken care of by the (transverse) equivalent photon flux factor, it has to be considered as a real photon in the sense that cross sections of subprocesses involving $\gamma(P^2)$ should be calculated as if $P^2 = 0$. In other words, the treatment and expressions for $f^{\gamma(P^2)}(x, Q^2)$ as on-shell transverse partons obeying the usual RG Q^2 -evolution equations (with the usual splitting functions of real photons, etc.) dictate an identification of the relevant resolved sub-cross-sections $f^{\gamma(P^2)}X \rightarrow X'$ with that of the real photon, $\hat{\sigma}(f^{\gamma(P^2)}X \rightarrow X') = \hat{\sigma}(f^\gamma X \rightarrow X')$. In particular, the calculation of $F_2^{\gamma(P^2)}(x, Q^2)$ requires the same photonic Wilson coefficient $C_\gamma(x)$ as for $P^2 = 0$, in contrast to what has been originally proposed [7, 8]. This allows to formulate similar boundary conditions in LO and NLO which give rise to perturbatively stable parton distributions, cross sections (i.e. also structure functions) of virtual photons $\gamma(P^2)$ as long as they are probed at scales $Q^2 \gg P^2$ where $Q^2 \equiv 4m_c^2, (p_T^{\text{jet}})^2$, etc., and typically

$P^2 \lesssim \frac{1}{10} Q^2$. It should be emphasized that only in this latter kinematic range $P^2 \ll Q^2$ is the whole concept of RG resummed parton distributions of (resolved) virtual photons appropriate and relevant. Parton distributions of virtual photons extracted recently from DIS ep dijet data are in good agreement with our (parameter-free) predictions.

Finally, we present simple analytic parametrizations of our predicted LO and NLO(DIS $_\gamma$) parton distributions of real photons. From these LO parametrizations one can easily obtain also the ones for a virtual photon which, within sufficient accuracy, may also be used in NLO. Our NLO(DIS $_\gamma$) parametrizations of the parton densities of the real photon can be easily transformed to the $\overline{\text{MS}}$ scheme according to eq. (4) which might be relevant for future NLO analyses of resolved photon contributions to hard processes where most NLO subprocesses have so far been calculated in the $\overline{\text{MS}}$ scheme.

A FORTRAN package containing our most recent parametrizations can be obtained by electronic mail on request.

Acknowledgements

This work has been supported in part by the ‘Bundesministerium für Bildung, Wissenschaft, Forschung und Technologie’, Bonn.

Appendix

Simple analytic parametrizations in LO and NLO of the ‘hadronic’ piece of the real and virtual photonic parton distributions, being proportional to $f^\pi(x, Q^2)$ in eqs. (13) and (25), respectively, are already known according to the recently published [21] parametrizations for $f^\pi(x, Q^2)$. Therefore we only need to parametrize the remaining ‘pointlike’ components in eqs. (13) and (25).

1. Parametrization of LO ‘pointlike’ photonic parton distributions

In LO the Q^2 dependence of the ‘pointlike’ $f_{pl}^\gamma(x, Q^2)$ term in (13) enters, apart from an overall $1/\alpha_s(Q^2)$ factor, merely via the combination $L \equiv \alpha_s(Q^2)/\alpha_s(\mu_{LO}^2)$ as is evident, for example, from eq. (2.12) of the first article in ref. [1]. Therefore, we prefer to parametrize the quantity $f_{pl}^\gamma(x, Q^2)$ in terms of

$$s \equiv \ln \frac{\ln [Q^2/(0.204 \text{ GeV})^2]}{\ln [\mu_{LO}^2/(0.204 \text{ GeV})^2]} \quad (\text{A.1})$$

where [23] $\mu_{LO}^2 = 0.26 \text{ GeV}^2$, which will later provide us a parametrization also for the virtual ‘pointlike’ component in (25). Our resulting ‘pointlike’ distributions in eq. (13) can be expressed by the following simple parametrizations, valid for $0.5 \lesssim Q^2 \lesssim 10^5 \text{ GeV}^2$ (i.e. $0.31 \lesssim s \lesssim 2.2$) and $10^{-5} \lesssim x < 1$:

$$\begin{aligned} \frac{1}{\alpha} x f_{pl}^\gamma(x, Q^2) &= \frac{9}{4\pi} \ln \frac{Q^2}{(0.204 \text{ GeV})^2} \left[s^\alpha x^a (A + B\sqrt{x} + C x^b) \right. \\ &\quad \left. + s^{\alpha'} \exp\left(-E + \sqrt{E' s^\beta \ln \frac{1}{x}}\right) \right] (1-x)^D \end{aligned} \quad (\text{A.2})$$

where for $f_{pl}^\gamma = u_{pl}^\gamma = \bar{u}_{pl}^\gamma$

$$\begin{aligned} \alpha &= 0.897, & \alpha' &= 2.626, \\ \beta &= 0.413, & & \\ a &= 2.137 - 0.310 \sqrt{s}, & b &= -1.049 + 0.113 s, \\ A &= -0.785 + 0.270 \sqrt{s}, & B &= 0.650 - 0.146 s, \\ C &= 0.252 - 0.065 \sqrt{s}, & D &= -0.116 + 0.403 s - 0.117 s^2, \\ E &= 6.749 + 2.452 s - 0.226 s^2, & E' &= 1.994 s - 0.216 s^2, \end{aligned} \quad (\text{A.3})$$

for $f_{pl}^\gamma = d_{pl}^\gamma = \bar{d}_{pl}^\gamma = s_{pl}^\gamma = \bar{s}_{pl}^\gamma$

$$\begin{aligned}
\alpha &= 1.084, & \alpha' &= 2.811, \\
\beta &= 0.960, \\
a &= 0.914, & b &= 3.723 - 0.968 s, \\
A &= 0.081 - 0.028 \sqrt{s}, & B &= -0.048 \\
C &= 0.094 - 0.043 \sqrt{s}, & D &= 0.059 + 0.263 s - 0.085 s^2, \\
E &= 6.808 + 2.239 s - 0.108 s^2, & E' &= 1.225 + 0.594 s - 0.073 s^2,
\end{aligned} \tag{A.4}$$

and for $f_{pl}^\gamma = g_{pl}^\gamma$

$$\begin{aligned}
\alpha &= 1.262, & \alpha' &= 2.024, \\
\beta &= 0.770, \\
a &= 0.081, & b &= 0.848 \\
A &= 0.012 + 0.039 \sqrt{s}, & B &= -0.056 - 0.044 s \\
C &= 0.043 + 0.031 s, & D &= 0.925 + 0.316 s, \\
E &= 3.129 + 2.434 s - 0.115 s^2, & E' &= 1.364 + 1.227 s - 0.128 s^2.
\end{aligned} \tag{A.5}$$

With these parametrizations at hand in terms of s in (A.1), the appropriate ones for the ‘pointlike’ distributions $f_{pl}^{\gamma(P^2)}(x, Q^2)$ of a virtual photon appearing in eq. (25) are simply given by the same expressions above where in (A.1) μ_{LO}^2 has to be replaced by $\tilde{P}^2 = \max(P^2, \mu_{LO}^2)$. As discussed in Sect. 3, these parametrizations can, within sufficient accuracy, also be used for the parton distribution of virtual photons in NLO.

2. Parametrization of NLO ‘pointlike’ photonic parton distributions

In NLO the Q^2 dependence of the ‘pointlike’ distributions of real photons in (13), $f_{pl}^\gamma(x, Q^2)$, can be easily described in terms of the following ‘effective’ logarithmic ratio

$$s \equiv \ln \frac{\ln [Q^2 / (0.299 \text{ GeV})^2]}{\ln [\mu_{\text{NLO}}^2 / (0.299 \text{ GeV})^2]} \tag{A.6}$$

to be evaluated for $\mu_{\text{NLO}}^2 = 0.40 \text{ GeV}^2$. Our NLO(DIS $_\gamma$) predictions can now be parametrized as the LO ones and are similarly valid for $0.5 \lesssim Q^2 \lesssim 10^5 \text{ GeV}^2$ (i.e. $0.14 \lesssim s \lesssim 2.38$) and $10^{-5} \lesssim x < 1$. For convenience we include now the NLO α_s in the r.h.s. of (A.2), i.e.

$$\frac{1}{\alpha} x f_{pl}^{\gamma}(x, Q^2) = \left[s^{\alpha} x^a (A + B\sqrt{x} + Cx^b) + s^{\alpha'} \exp\left(-E + \sqrt{E' s^{\beta} \ln \frac{1}{x}}\right) \right] (1-x)^D \quad (\text{A.7})$$

where for $f_{pl}^{\gamma} = u_{pl}^{\gamma} = \bar{u}_{pl}^{\gamma}$

$$\begin{aligned} \alpha &= 1.051, & \alpha' &= 2.107, \\ \beta &= 0.970, \\ a &= 0.412 - 0.115 \sqrt{s}, & b &= 4.544 - 0.563 s, \\ A &= -0.028 \sqrt{s} + 0.019 s^2, & B &= 0.263 + 0.137 s, \\ C &= 6.726 - 3.264 \sqrt{s} - 0.166 s^2, & D &= 1.145 - 0.131 s^2, \\ E &= 4.122 + 3.170 s - 0.598 s^2, & E' &= 1.615 s - 0.321 s^2, \end{aligned} \quad (\text{A.8})$$

for $f_{pl}^{\gamma} = d_{pl}^{\gamma} = \bar{d}_{pl}^{\gamma} = s_{pl}^{\gamma} = \bar{s}_{pl}^{\gamma}$

$$\begin{aligned} \alpha &= 1.043, & \alpha' &= 1.812, \\ \beta &= 0.457, \\ a &= 0.416 - 0.173 \sqrt{s}, & b &= 4.489 - 0.827 s, \\ A &= -0.010 \sqrt{s} + 0.006 s^2, & B &= 0.064 + 0.020 s \\ C &= 1.577 - 0.916 \sqrt{s}, & D &= 1.122 - 0.093 s - 0.100 s^2, \\ E &= 5.240 + 1.666 s - 0.234 s^2, & E' &= 1.284 s \end{aligned} \quad (\text{A.9})$$

and for $f_{pl}^{\gamma} = g_{pl}^{\gamma}$

$$\begin{aligned} \alpha &= 0.901, & \alpha' &= 1.773, \\ \beta &= 1.666, \\ a &= 0.844 - 0.820 \sqrt{s} & b &= 2.302 - 0.474 s \\ A &= 0.194 & B &= -0.324 + 0.143 s \\ C &= 0.330 - 0.177 s, & D &= 0.778 + 0.502 s - 0.154 s^2 \\ E &= 2.895 + 1.823 s - 0.441 s^2, & E' &= 2.344 - 0.584 s. \end{aligned} \quad (\text{A.10})$$

References

- [1] M. Glück, E. Reya, and A. Vogt, *Phys. Rev.* **D45**, 3986 (1992); *ibid.* **D46**, 1973 (1992).
- [2] L.E. Gordon and J.K. Storrow, *Z. Phys.* **C56**, 307 (1992); *Nucl. Phys.* **B489**, 405 (1997); K. Hagiwara et al., *Phys. Rev.* **D51**, 3197 (1995).
- [3] P. Aurenche, M. Fontannaz, and J.-P. Guillet, *Z. Phys.* **C64**, 621 (1994).
- [4] M. Erdmann, ‘The Partonic Structure of the Photon’, Springer Tracts in Modern Physics **138** (1997).
- [5] A. Vogt, Proceedings of the Photon ’97 Conference, Egmond aan Zee, May 1997, eds. A. Buijs and F.C. Erne, World Scientific (1998), p. 3 (hep-ph/9709345).
- [6] Recent experimental results can be found in the Proceedings of the Photon ’97 Conference, Egmond aan Zee, May 1997, eds. A. Buijs and F.C. Erne, World Scientific (1998).
- [7] T. Uematsu and T.F. Walsh, *Phys. Lett.* **101B**, 263 (1981); *Nucl. Phys.* **B199**, 93 (1982); W. Ibes and T.F. Walsh, *Phys. Lett.* **B251**, 450 (1990).
- [8] G. Rossi, *Phys. Rev.* **D29**, 852 (1984); UC San Diego report UCSD-10P10-227 (unpublished).
- [9] F.M. Borzumati and G.A. Schuler, *Z. Phys.* **C58**, 139 (1993).
- [10] M. Glück, E. Reya, and M. Stratmann, *Phys. Rev.* **D51**, 3220 (1995).
- [11] G.A. Schuler and T. Sjöstrand, *Z. Phys.* **C68**, 607 (1995); *Phys. Lett.* **B376**, 193 (1996).
- [12] M. Drees and R.M. Godbole, *Phys. Rev.* **D50**, 3124 (1994)

- [13] M. Stratmann, talk presented at the Workshop on Photon Interactions and the Photon Structure, Lund, Sept. 1998, (Univ. Durham report DTP/98/80, hep-ph/9811260).
- [14] M.L. Utley, ZEUS Collab., Proceedings of the Int. Europhysics Conf. on HEP '95, Brussels, 1995, eds. J. Lemonne et al., World Scientific, p. 570 (hep-ex/9508016); C. Adloff et al., H1 Collab., *Phys. Lett.* **B415**, 418 (1997); DESY 98-076 (hep-ex/9806029); Paper 544, submitted to the 29th Int. Conf. on HEP ICHEP98, Vancouver, July 1998; DESY-98-205 (hep-ex/9812024).
- [15] M. Glück, E. Reya, and M. Stratmann, *Phys. Rev.* **D54**, 5515 (1996).
- [16] D. de Florian, C. Garcia Canal, and R. Sassot, *Z. Phys.* **C75**, 265 (1997); J. Chýla and J. Cvach, Proceedings of the 1995/96 Workshop on Future Physics at HERA, eds. G. Ingelman, A. DeRoeck, and R. Klanner, DESY 1996, vol. 1, p. 545.
- [17] M. Klasen, G. Kramer, and B. Pötter, *Eur. Phys. J.* **C1**, 261 (1998);
G. Kramer and B. Pötter, *Eur. Phys. J.* **C5**, 665 (1998);
B. Pötter, DESY 98-071 (hep-ph/9806437).
- [18] H. Jung, *Comp. Phys. Comm.* **86**, 147 (1995).
- [19] M. Glück, E. Reya, and A. Vogt, *Z. Phys.* **C53**, 127 (1992); *Phys. Lett.* **B306**, 391 (1993); *Z. Phys.* **C67**, 433 (1995).
- [20] M. Glück, E. Reya, and A. Vogt, *Z. Phys.* **C53**, 651 (1992).
- [21] M. Glück, E. Reya, and I. Schienbein, Univ. Dortmund report DO-TH 99/01 (hep-ph/9903288), *Eur. Phys. J.*, to appear.
- [22] M. Glück, E. Reya, and M. Stratmann, *Eur. Phys. J.* **C2**, 159 (1998).
- [23] M. Glück, E. Reya, and A. Vogt, *Eur. Phys. J.* **C5**, 461 (1998).
- [24] W.A. Bardeen, A.J. Buras, D.W. Duke, and T. Muta, *Phys. Rev.* **D18**, 3998 (1978).

- [25] W.A. Bardeen and A.J. Buras, *Phys. Rev.* **D20**, 166 (1979); **21**, 2041 (1980) (E).
- [26] M. Glück, E. Reya, and A. Vogt, *Phys. Rev.* **D48**, 116 (1993).
- [27] Particle Data Group, C. Caso et al., *Eur. Phys. J.* **C3**, 1 (1998).
- [28] Yu.M. Antipov et al., *Z. Phys.* **C42**, 185 (1989).
- [29] Ch. Berger and W. Wagner, *Phys. Rep.* **146**, 1 (1987);
H. Kolanoski and P. Zerwas, DESY-87-175, ‘High Energy Electron–Positron Physics’,
eds. A. Ali and P. Söding (World Scientific, Singapore, 1988);
B.L. Ioffe, V.A. Khoze, and L.N. Lipatov, ‘Hard Processes’ (North–Holland, 1984).
- [30] E. Witten, *Nucl. Phys.* **B104**, 445 (1976);
M. Glück and E. Reya, *Phys. Lett.* **83B**, 98 (1979).
- [31] M. Glück, E. Reya, and M. Stratmann, *Nucl. Phys.* **B422**, 37 (1994).
- [32] E. Laenen, S. Riemersma, J. Smith, and W.L. van Neerven, *Phys. Rev.* **D49**, 5753
(1994); E. Laenen and S. Riemersma, Proceedings of the Photon ’95 Conference,
Sheffield, April 1995 (hep–ph/9505230); *Phys. Lett.* **B376**, 169 (1996).
- [33] Ch. Berger et al., PLUTO Collab., *Phys. Lett.* **142B**, 111 (1984); *Nucl. Phys.* **B281**,
365 (1987);
W. Bartel et al., JADE Collab., *Z. Phys.* **C24**, 231 (1984);
M. Althoff et al., TASSO Collab., *Z. Phys.* **C31**, 527 (1986);
S.K. Sahu et al., AMY Collab., *Phys. Lett.* **B346**, 208 (1995); T. Kojima et al., AMY
Collab., *Phys. Lett.* **B400**, 395 (1997);
K. Muramatsu et al., TOPAZ Collab., *Phys. Lett.* **B332**, 477 (1994);
K. Ackerstaff et al., OPAL Collab., *Z. Phys.* **C74**, 33 (1997); *Phys. Lett.* **B411**, 387
(1997); *ibid.* **B412**, 225 (1997);
P. Abreu et al., DELPHI Collab., *Z. Phys.* **C69**, 223 (1996);
F. Kapusta et al., DELPHI Collab., HEP ’97 Conference, Jerusalem, August 1997,
contribution 416; A. Finch et al., ALEPH Collab., *ibid.*, contribution 607; Photon ’97

- Conference, Egmond aan Zee, May 1997; ICHEP '98 Conference, Vancouver, July 1998, Abstract No. 898;
- M. Acciarri et al., L3 Collab., *Phys. Lett.* **B436**, 403 (1998).
- [34] T. Ahmed et al., H1 Collab., *Nucl. Phys.* **B445**, 195 (1995);
C. Adloff et al., H1 Collab., DESY 98-148 (hep-ex/9810020), *Eur. Phys. J.*, to appear.
- [35] L.L. Frankfurt and E.G. Gurvich, Univ. Tel Aviv report 'Momentum Sum Rules in QCD for a Photon Target', May 1995 (hep-ph/9505406), unpublished; *J. Phys.* **G22**, 903 (1996); *Phys. Lett.* **B386**, 379 (1996).
- [36] M. Glück and E. Reya, *Phys. Lett.* **B443**, 298 (1998).
- [37] H. Burkhardt and B. Pietrzyk, *Phys. Lett.* **B356**, 398 (1995).
- [38] V.M. Budnev, I.F. Ginzburg, G.V. Meledin, and V.G. Serbo, *Phys. Rep.* **15**, 181 (1975);
S. Frixione, M.L. Mangano, P. Nason, and G. Ridolfi, *Phys. Lett.* **B319**, 339 (1993).
- [39] Ch. Berger et al., PLUTO Collab., *Phys. Lett.* **142B**, 119 (1984).

Figure Captions

- Fig. 1** Comparison of our radiatively generated LO and NLO(DIS $_{\gamma}$) predictions for $F_2^{\gamma}(x, Q^2)$, based on the valence-like parameter-free VMD input in eq. (9), with the data of ref. [33]. For our comparison the GRV $_{\gamma}$ [1] results are shown as well. In both cases, the charm contribution has been added, in the relevant kinematic region $W \geq 2m_c$, according to eqs. (15) and (16).
- Fig. 2** Comparison of our predicted LO and NLO(DIS $_{\gamma}$) distributions $u^{\gamma} = \bar{u}^{\gamma}$, $d^{\gamma} = \bar{d}^{\gamma}$ and g^{γ} at $Q^2 = 10 \text{ GeV}^2$ with the LO/NLO GRV $_{\gamma}$ densities [1], the LO SaS 1D and 2D [11] and the NLO AFG [3] distributions. The ‘hadronic’ (pionic) components of our total LO and NLO results in eq. (11) are displayed by the dashed curves.
- Fig. 3** Detailed small- x (as well as large- x) behavior and predictions of our radiatively generated $u^{\gamma} = \bar{u}^{\gamma}$ and g^{γ} distributions in LO and NLO(DIS $_{\gamma}$) at fixed values of Q^2 . The dashed-dotted curves show the hadronic NLO contribution f_{had}^{γ} to $f^{\gamma} = f_{\text{pl}}^{\gamma} + f_{\text{had}}^{\gamma}$ in eq. (11). The valence-like inputs at $Q^2 = \mu_{\text{LO, NLO}}^2$, according to eq. (9), are shown by the lowest curves referring to μ^2 . For comparison we show the steeper NLO GRV $_{\gamma}$ [1] expectations as well. The results have been multiplied by the number indicated in brackets.
- Fig. 4** Comparison of our LO and NLO predictions for xg^{γ} at $Q^2 \equiv \langle (p_T^{\text{jet}})^2 \rangle = 75 \text{ GeV}^2$ with HERA(H1) measurements [34]. The GRV $_{\gamma}$ and SaS expectations are taken from refs. [1] and [11], respectively.
- Fig. 5** LO and NLO predictions for $F_{\text{eff}}^{\gamma(P^2)} \equiv F_2^{\gamma(P^2)} + \frac{3}{2}F_L^{\gamma(P^2)}$. The charm contributions have been calculated according to eqs. (15), (16) and (28), and the ‘resolved’ charm contribution to $F_L^{\gamma(P^2)}$ is calculated analogously as in (16) with $f_L^{\gamma*(Q^2)g^{\gamma} \rightarrow h\bar{h}}(x, Q^2)$ being given by eq. (28) with $e_c^4\alpha \rightarrow e_c^2\alpha_s(\mu_F^2)/6$. The ‘box’ is defined by eqs. (26) and (27). The PLUTO data are taken from ref. [39].

Fig. 6a LO and NLO predictions for the x dependence of the virtual photon structure function $F_2^{\gamma(P^2)}$ at $Q^2 = 10 \text{ GeV}^2$ and various fixed values of $P^2 \ll Q^2$, neglecting any heavy quark contribution. For comparison we also show the NLO GRS [10] results as well as the predictions for a real ($P^2 = 0$) photon. Notice that the dotted curve for $P^2 = 0$ referred to as GRS obviously coincides with the GRV_γ result [1]. The results have been multiplied by the number indicated in brackets.

Fig. 6b As in fig. 6a but at $Q^2 = 100 \text{ GeV}^2$.

Fig. 7a Comparison of our predicted LO and NLO(DIS_γ) distributions of the virtual photon at $Q^2 = 10 \text{ GeV}^2$ and various fixed values of $P^2 \ll Q^2$ with the GRS densities [10]. The curves refer from top to bottom to $P^2 = 0, 0.2$ and 1 GeV^2 , respectively. The results for the real photon ($P^2 = 0$) are very similar to the ones in fig. 2 where the GRV_γ curves practically coincide with GRS.

Fig. 7b Our LO distributions as in fig. 7a compared with the ones of SaS [11].

Fig. 8 LO and NLO predictions for the up-quark and gluon distributions of a virtual photon $\gamma(P^2)$ at $Q^2 = 10 \text{ GeV}^2$. For comparison the results for the real photon ($P^2 = 0$) are shown as well. The NLO ‘hadronic’ contribution in (25) is also shown separately. The GRS expectations are taken from ref. [10]. The DIS_γ results for $u^{\gamma(P^2)}$ can be easily converted to the $\overline{\text{MS}}$ scheme with the help of eq. (4), whereas $g^{\gamma(P^2)}$ remains the same in both schemes. The results have been multiplied by the numbers indicated in brackets.

Fig. 9 As in fig. 8 but at $Q^2 = 100 \text{ GeV}^2$.

Fig. 10 Predictions for the LO effective parton density $x\tilde{f}^{\gamma(P^2)}(x, Q^2)$, defined in eq. (29), at the scale $Q^2 \equiv (p_T^{\text{jet}})^2 = 85 \text{ GeV}^2$ and at two fixed values of x . The H1 data [14] have been extracted from DIS ep dijet production. The solid curves refer to our predictions in the theoretically legitimate region $P^2 \ll Q^2 \equiv (p_T^{\text{jet}})^2$, whereas the dashed curves extend into the kinematic region of larger P^2 approaching Q^2

where the concept of parton distributions of virtual photons is not valid anymore (see text).

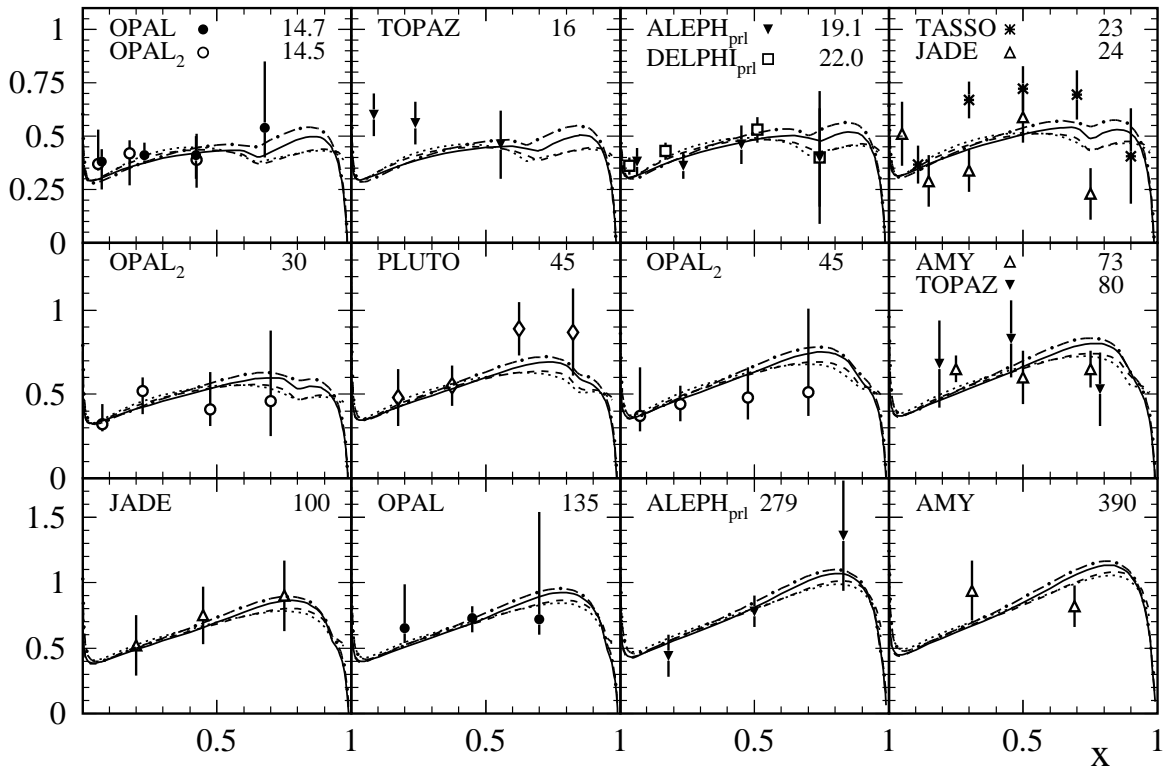
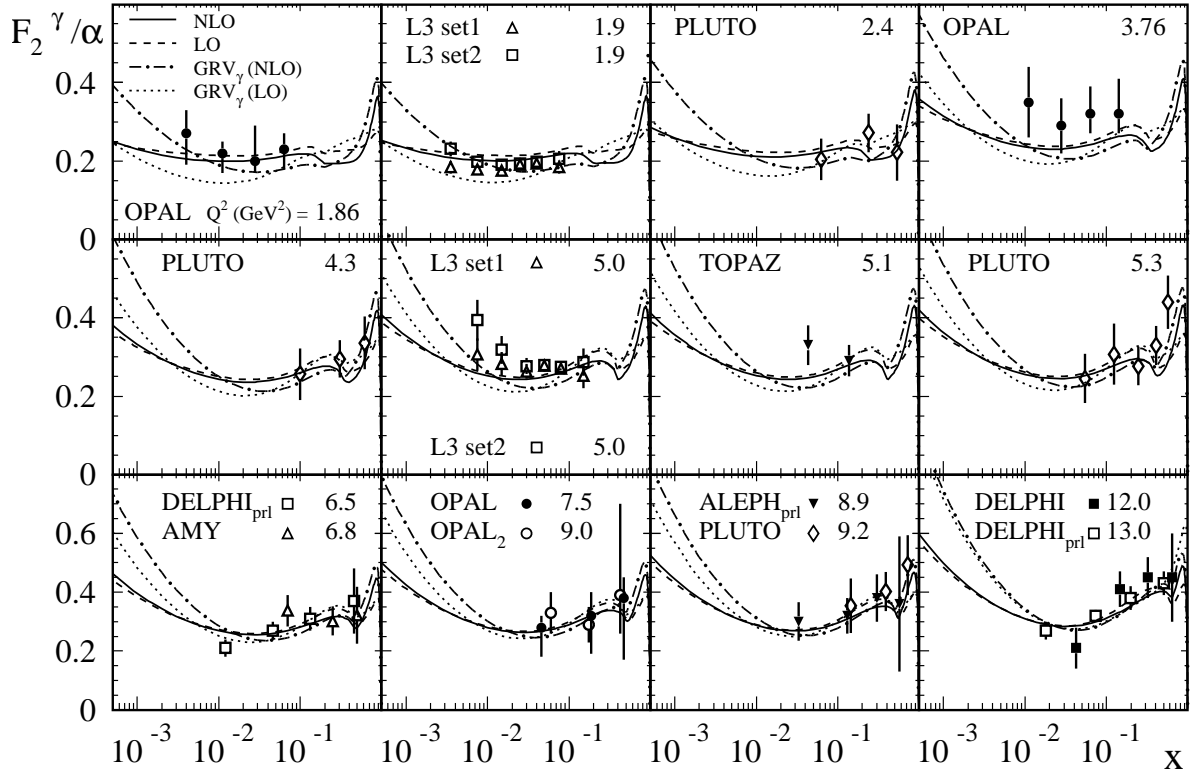


Fig. 1

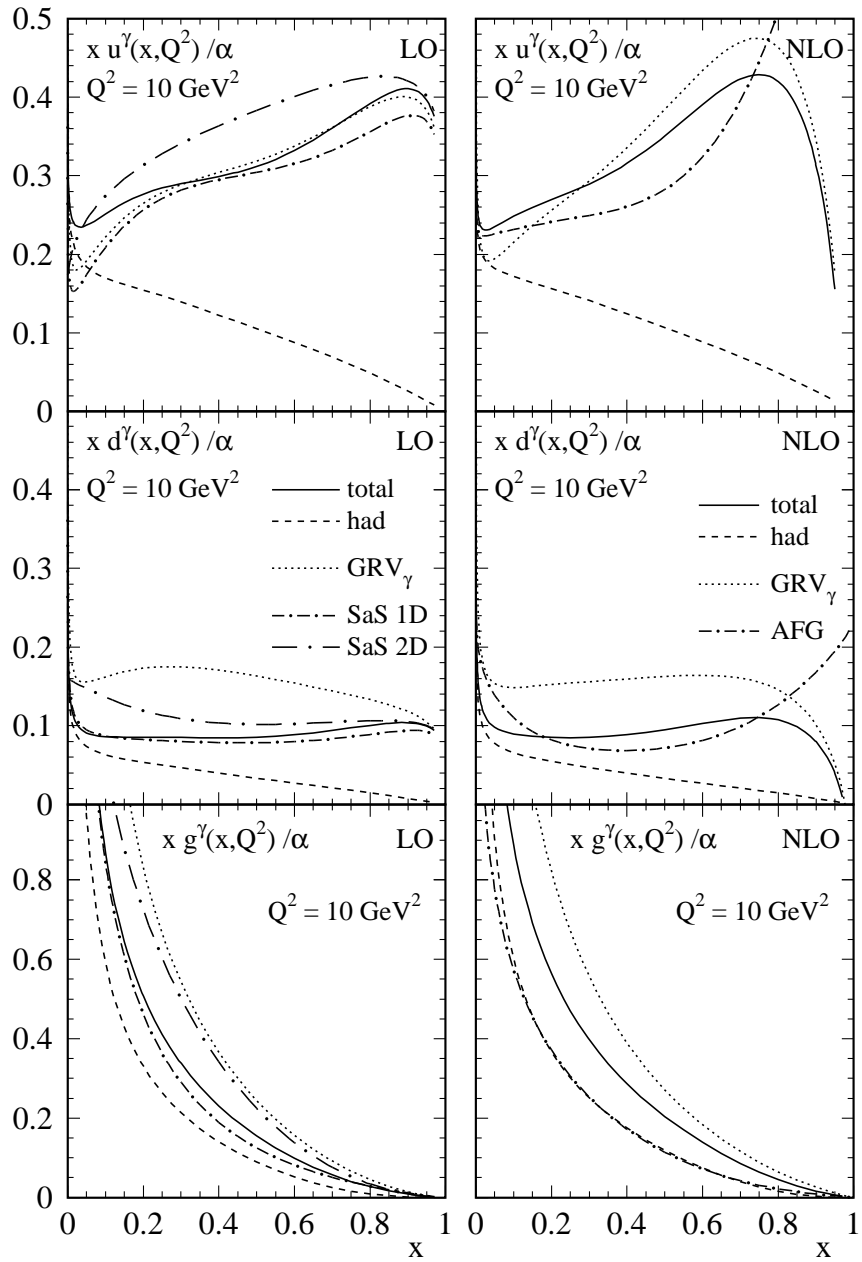
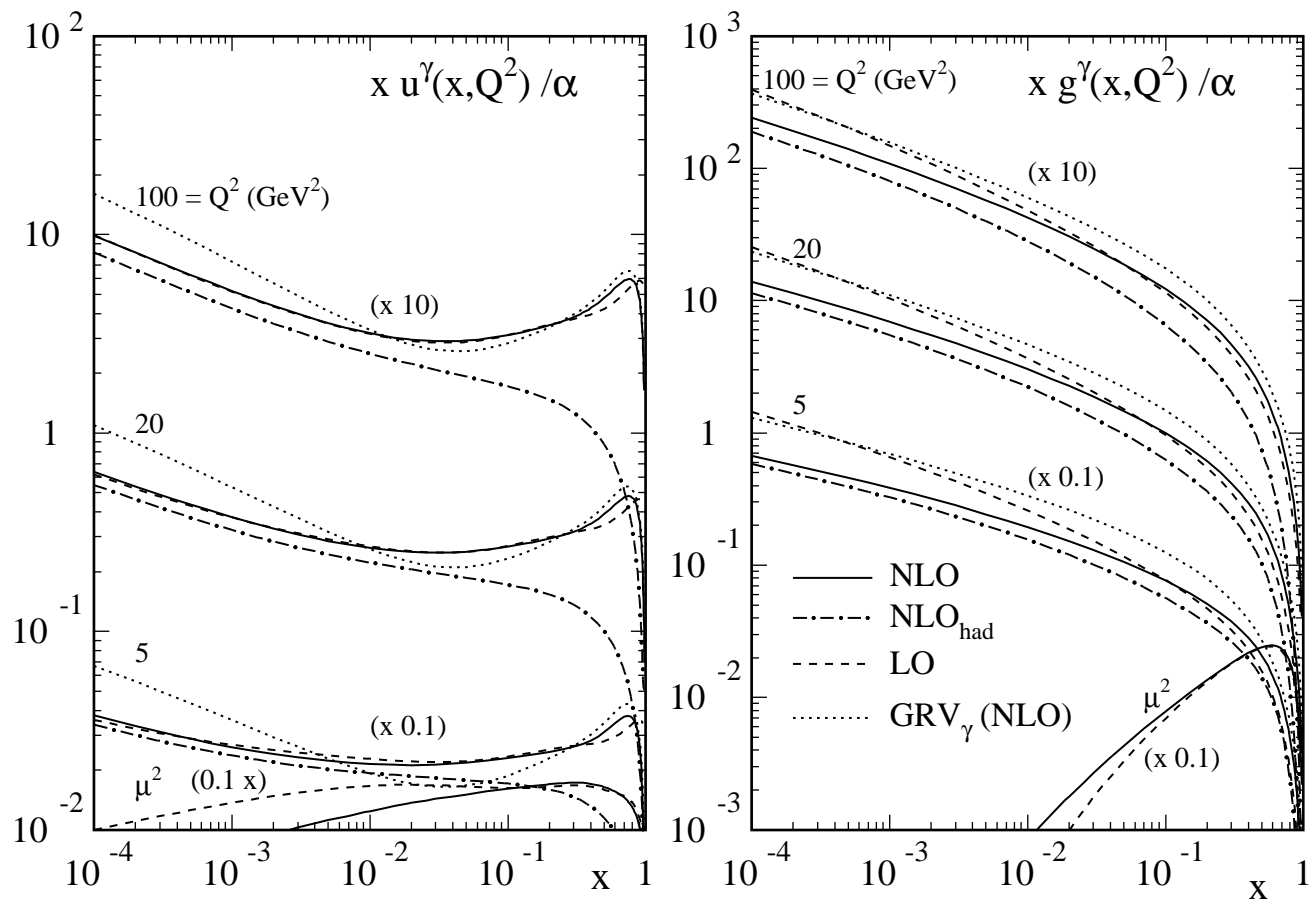


Fig. 2

Fig. 3



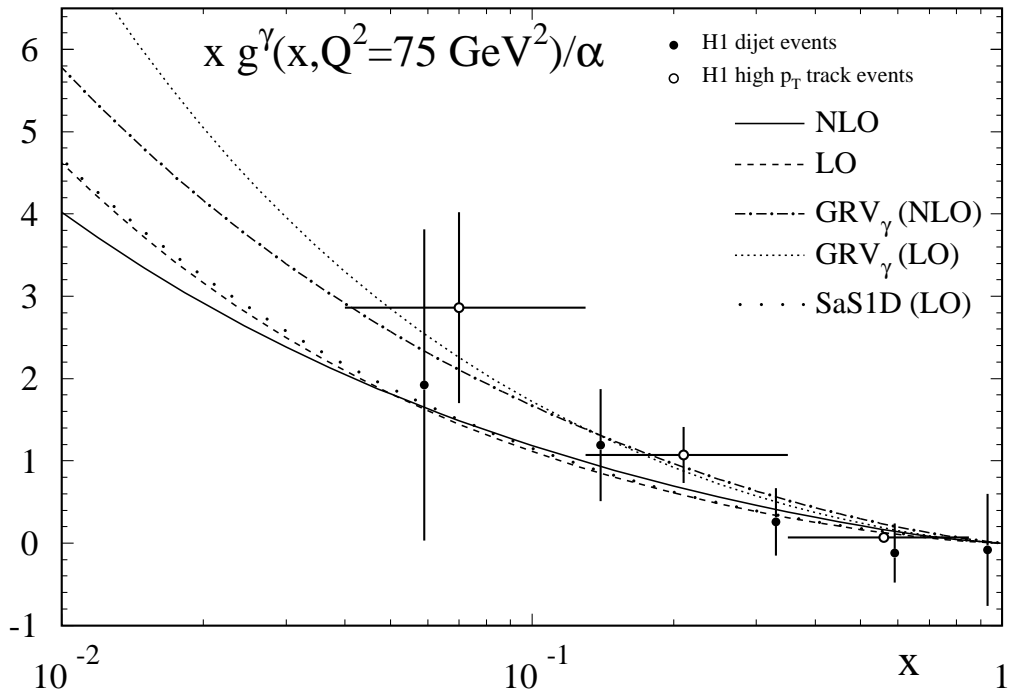


Fig. 4

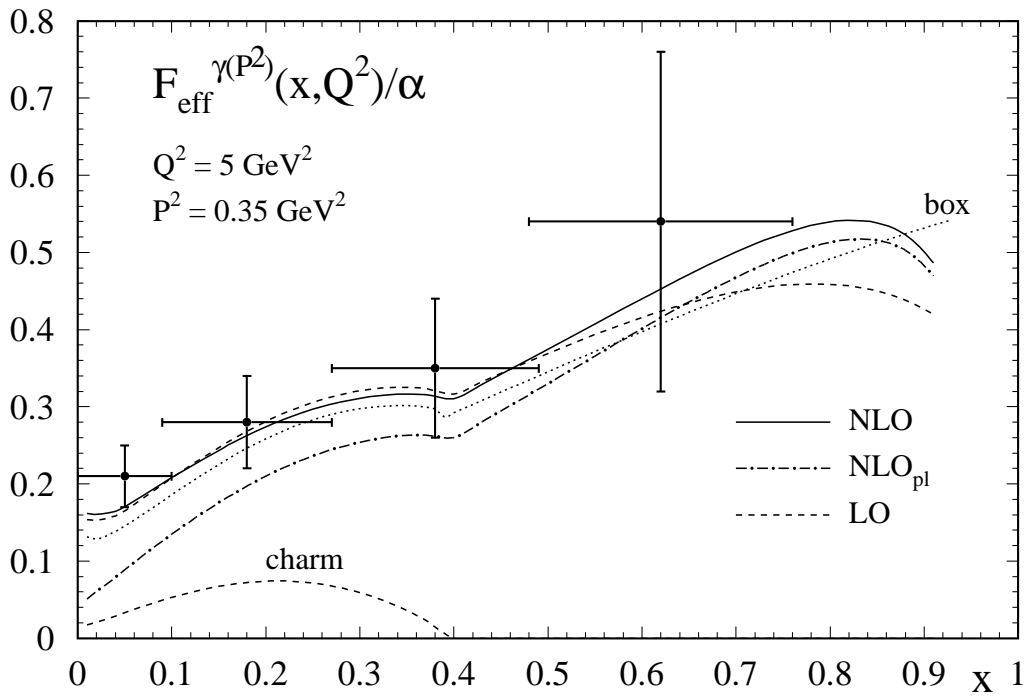


Fig. 5

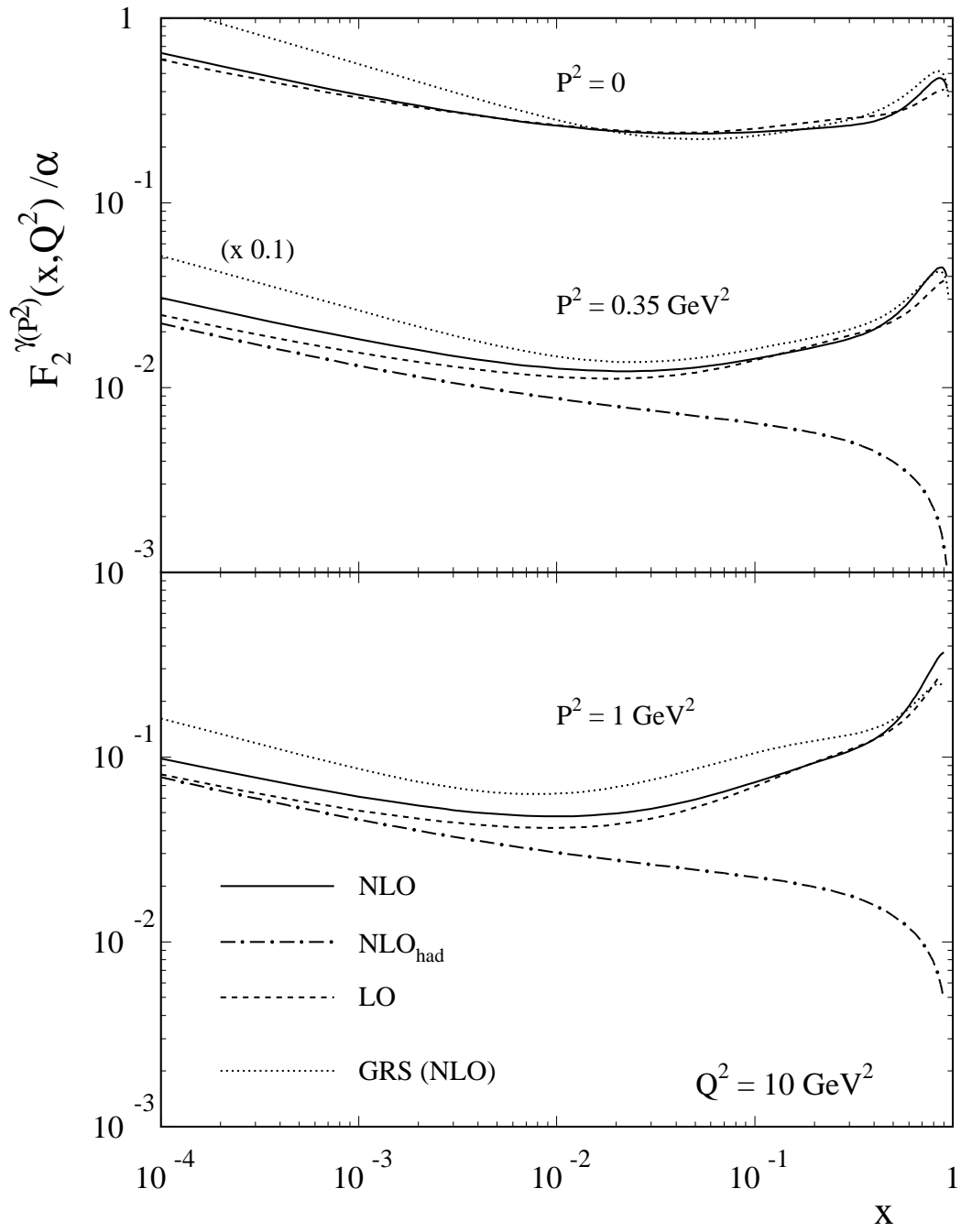


Fig. 6a

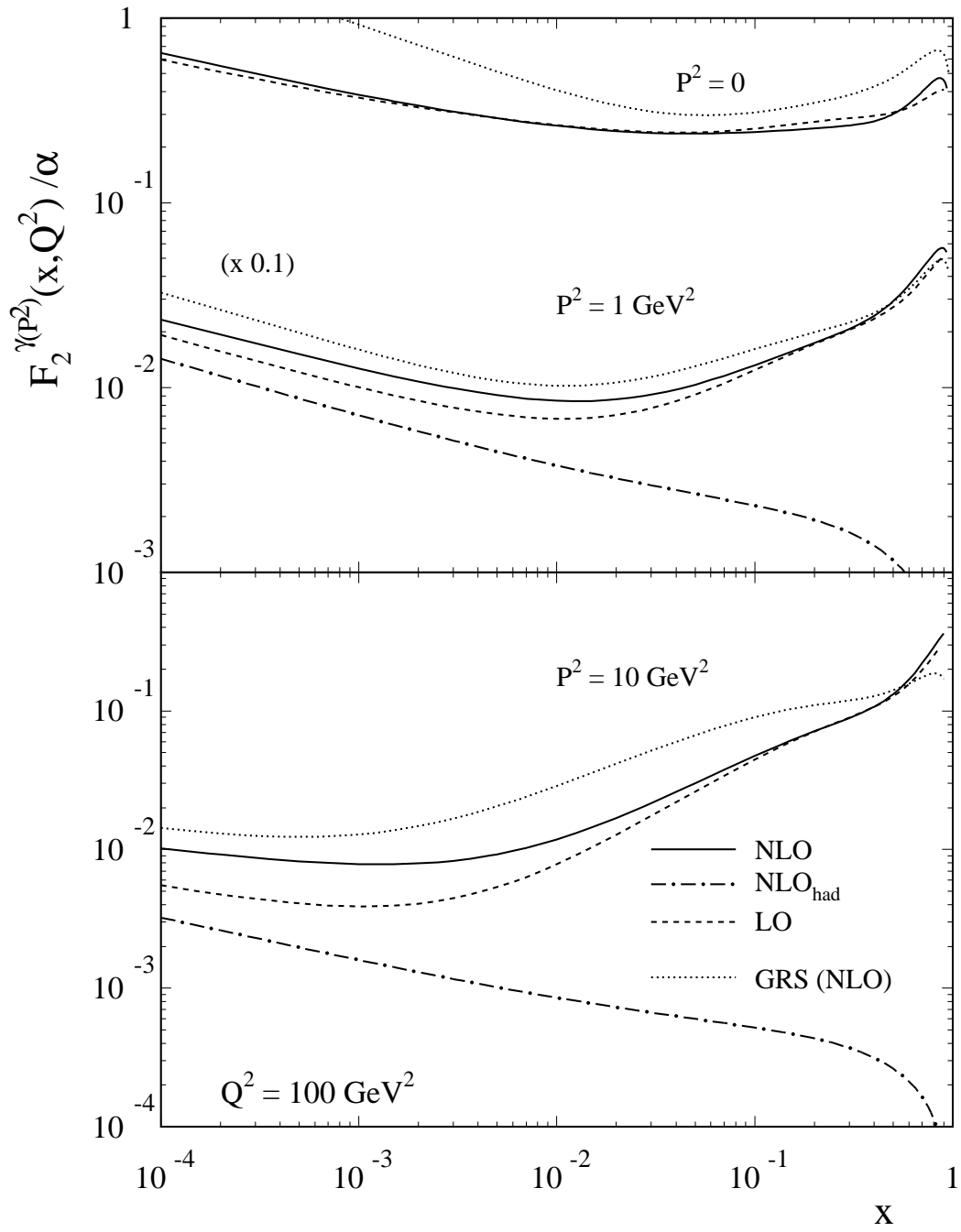


Fig. 6b

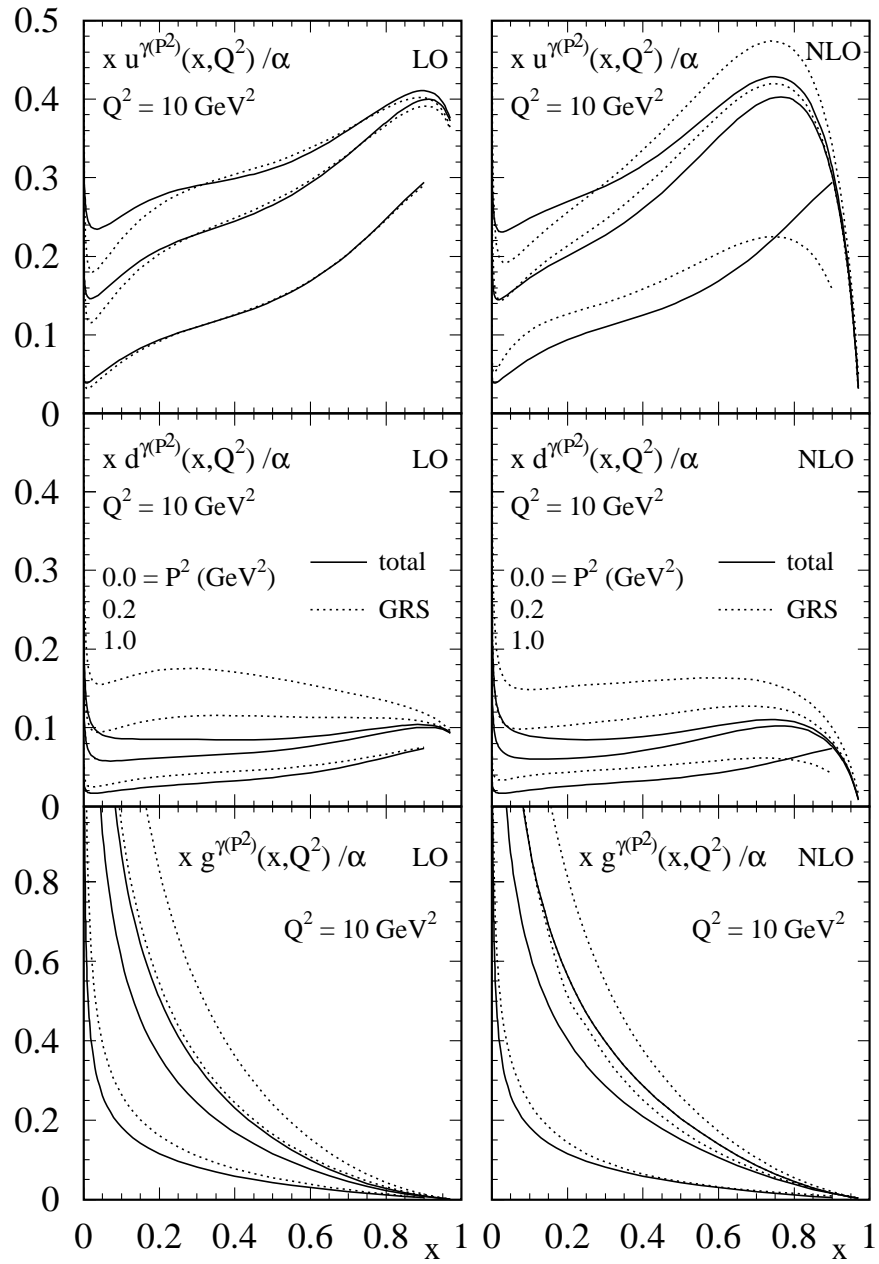


Fig. 7a

Fig. 7b

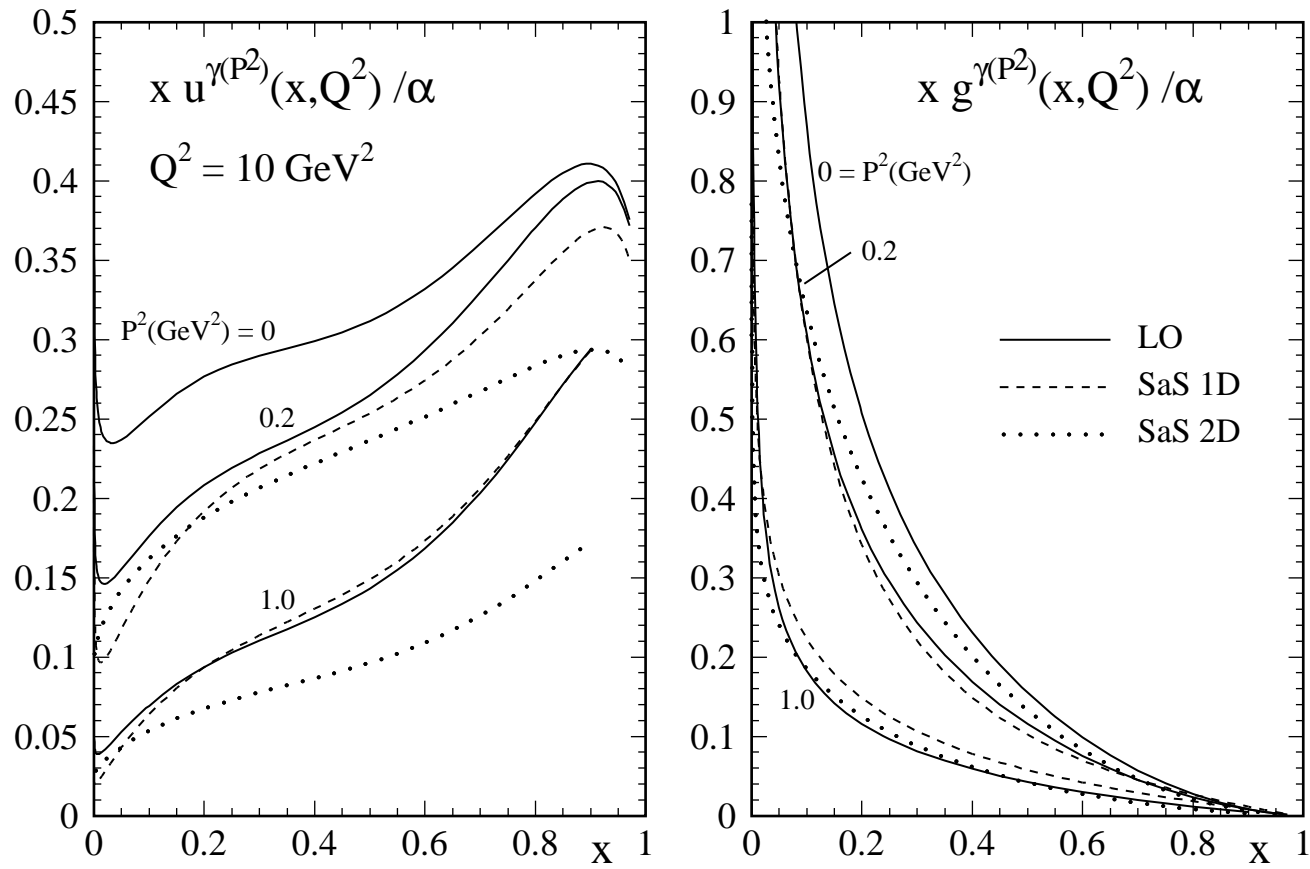


Fig. 8

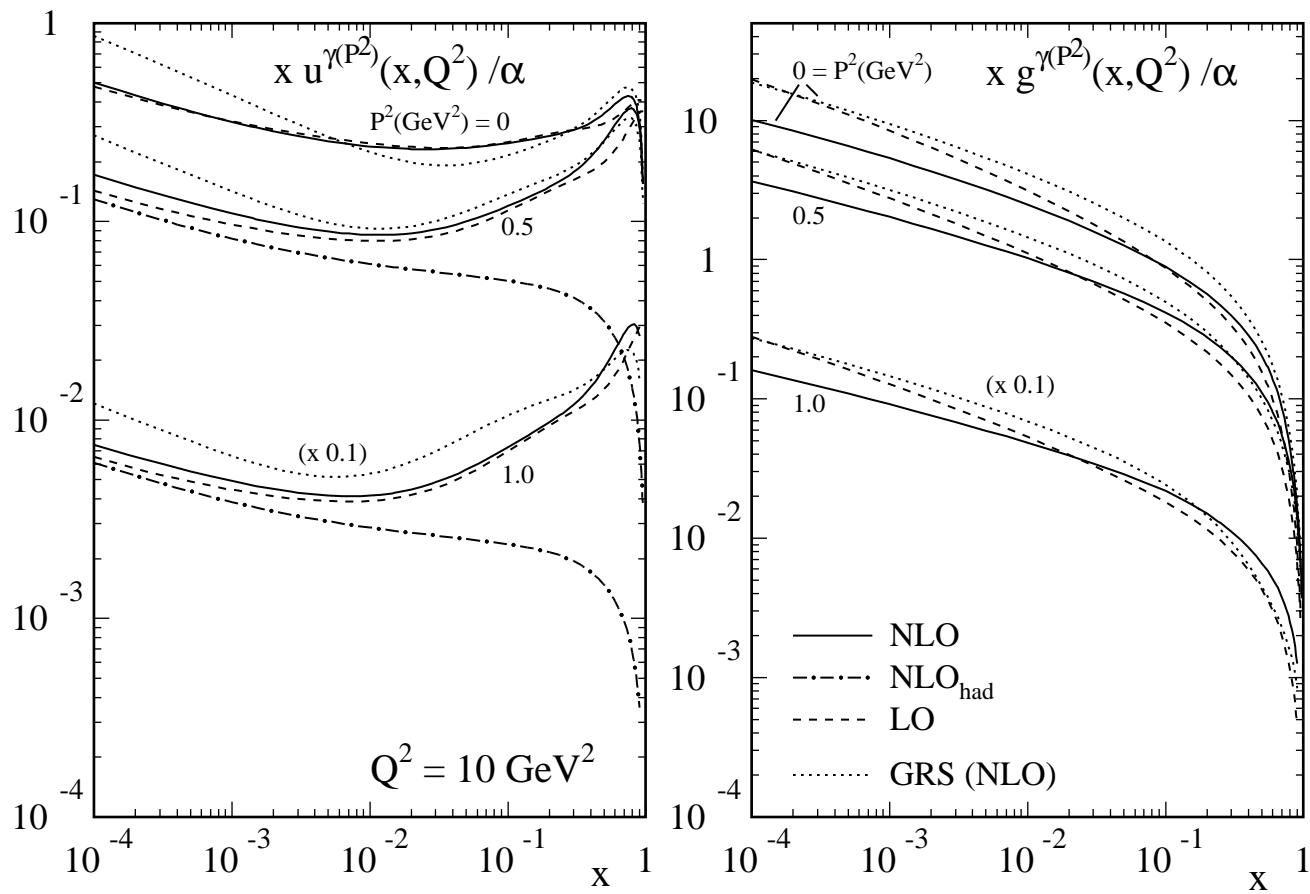
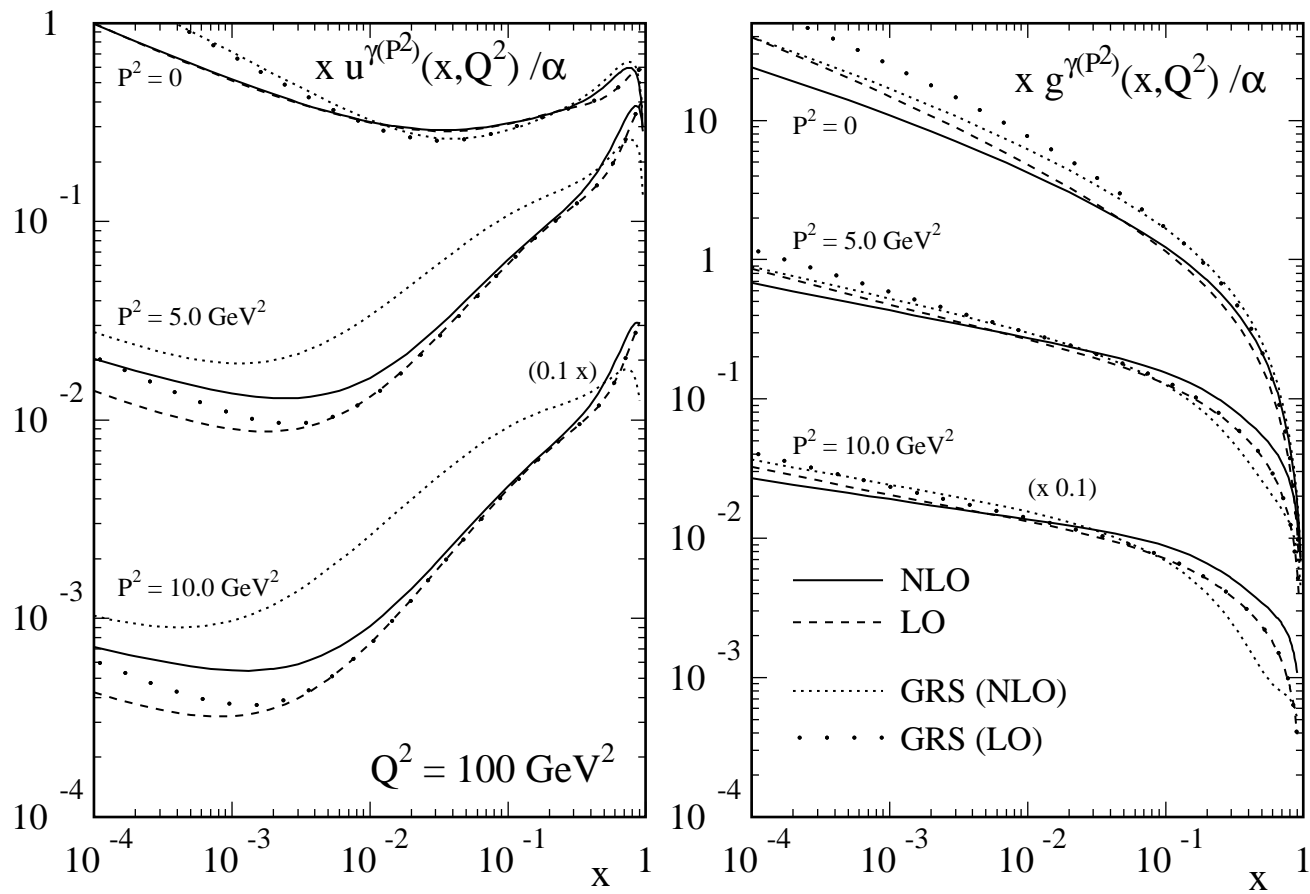


Fig. 9



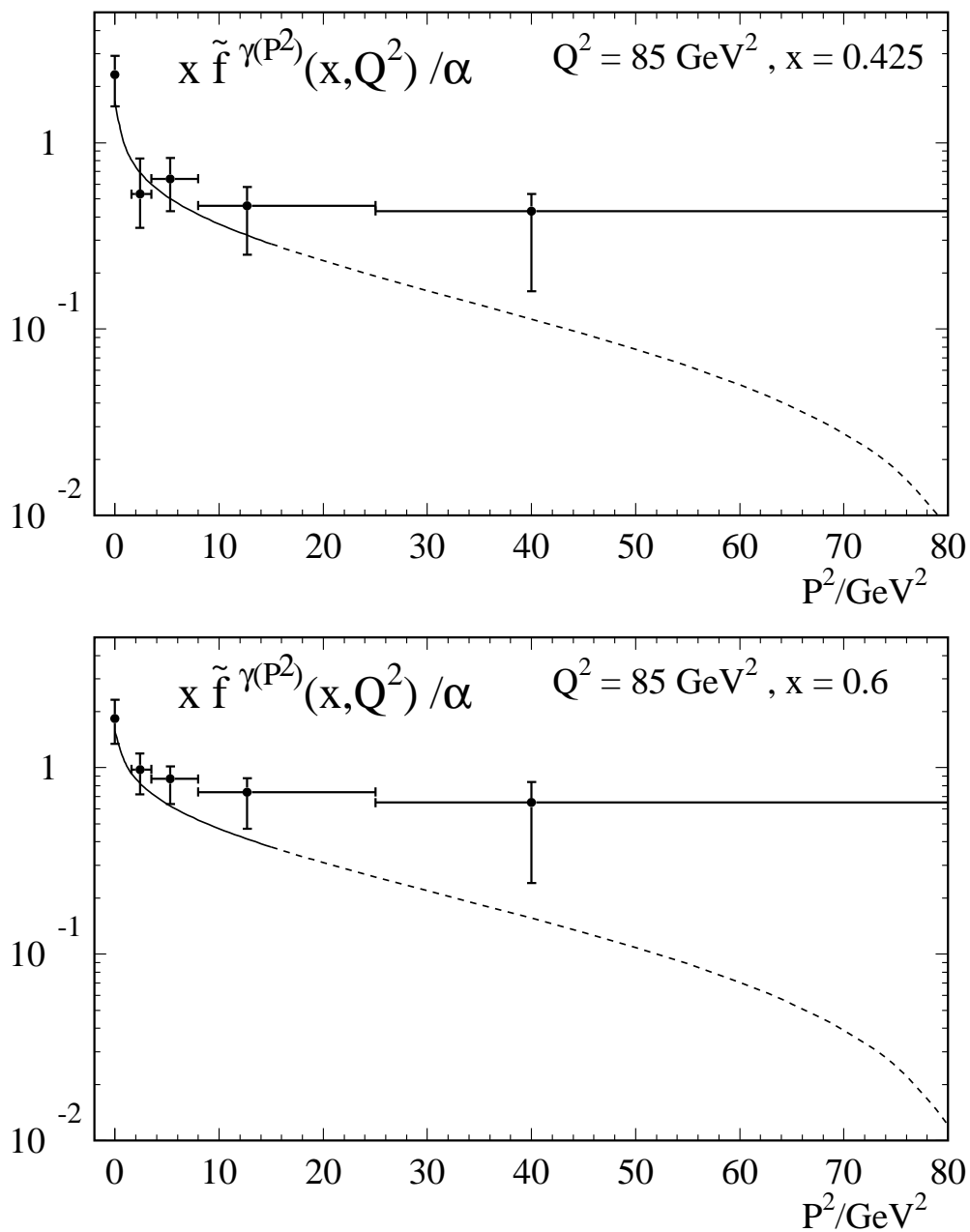


Fig. 10